university of groningen

faculty of science and engineering

Characterization of the shower profile of extensive air showers in the atmosphere in the TeV energy range

Morgan Abdoelrazak

First supervisor: Dr. M. Vecchi
Daily supervisor: A.G. Delgado Giler
Second reader: Dr J. Noel-Storr

July 8, 2022

Contents

Acknowledgments

I would like to thank my supervisor, Manuela Vecchi, for motivating me to do this projects. Her advice and support towards me truly has made me want to continue and see this through to the end. The guidance given throughout this process has made me think in new and intuitive ways and allowed me to develop further.
In addition I want to thank Andrés G. Delgado Giler for not only providing the data used during this project, but also for always having his door open and taking the time to explain concepts or theory I did not understand and helping me whenever I got stuck on something throughout the research process.

1 Introduction

The longitudinal development of air showers in the atmosphere is an essential tool to study the highest energy cosmic rays, with energies above 10^{15} eV, where space-based detection is not possible due to the extremely low fluxes. The shower maximum X_{max} is a powerful observable to study cosmic rays because it is connected to the energy and mass composition of the primary cosmic-ray particle. In this project, we use simulated showers generated with the CONEX simulation package to characterise the shower profile for different species (photons, protons and iron nuclei) and different energies (10 TeV, 50 TeV, 100 TeV, 300 TeV). This work aims at characterizing the shower profile in the TeV range, and fits in the current efforts on the astroparticle physics group at Kapteyn institute, in view of the work on cosmic-ray identification with future observatories. We use two trial functions to characterise the longitudinal development of the shower profile and to obtain the shower maximum X_{max}. In particular, we use the so-called Gaisser-Hillar function and the Gaussian in age function.
The goal of this study is to investigate which function describes better the shower profiles of the different particles and at the different energies. Moreover, we test the stability of the results and the sensitivity of the method to the tails of the profile by first fitting over the whole range in the atmospheric depth and later fitting over a given range around the shower maximum. This latter test is important to understand how each of these fit functions is sensitive to the behaviour in the very high and very low regions of the atmosphere, which are generally those with the largest uncertainties, due to the intrinsic capabilities of the detection technique.
This manuscript is organised as follows: Section 2 provides a brief overview of the process of the extensive air showers in the atmosphere and explains the relevant parameters that characterise the shower profile. Section 3 describes the methods that were used in this project, and in particular, the analysis framework is described, together with two fit functions that are used to characterise the shower shape. Section 4 describes the results, and the conclusions are addressed in section 5. Additional plots are shown in the appendix.

2 Extensive Air Showers in the atmosphere

Extensive air showers (EAS) are cascades of particles initiated by the interaction of a high-energy particle, also referred to as primary particles, at the top of the atmosphere causing a chain reaction of secondary particles creating a particle shower. These showers contain an electromagnetic, a hadronic, a muonic and a neutrino component. It is important to note that all primary particles discussed throughout this dissertation originate from cosmic rays. Cosmic rays are defined as charged particles or electrons from galactic origin, with high-energy particles originating from extra-galactic astrophysical objects. About 90% of these particles consists of protons, 9% bare helium nuclei, 1% bare nuclei of heavier elements such as Carbon and Iron, and the remainder consisting of electrons and high energy photons. Depending on the origin these particles can have an energy ranging between 10^9 eV and 10^{20} eV [1].
The energy spectrum of the cosmic rays can be seen in figure 1 and follows a smooth power-law spectrum, $F(E) = c \cdot E^{-\alpha}$, where c represents a constant. The so-called knee appears at about $3 \cdot 10^6$ GeV, where the spectrum steepens from $\alpha = 2.7$ to $\alpha = 3.1$. The so-called ankle appears at about $3 \cdot 10^9$ GeV, where the spectrum becomes flatter again. The common understanding is that cosmic rays below the knee are accelerated by supernova remnants. This generally accepted scenario derives from observing gamma rays up to 10 TeV, which have been detected from sources in the vicinity of well-known supernova remnants. Since TeV gamma rays can be produced by the interaction of accelerated cosmic rays in these sources, these observations indicate that these are sources of cosmic rays' acceleration. Cosmic rays of energies above the knee are thus certainly of extragalactic origin because particles of these energies cannot be confined in our galaxy.

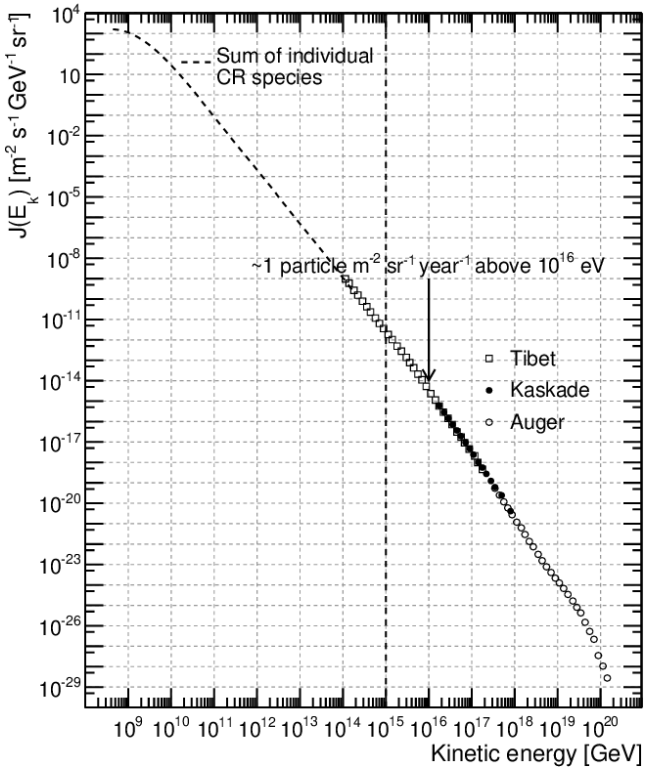

Figure 1: Energy spectrum of primary cosmic rays, with the dashed line (10^9 to 10^{14} eV) representing the energy spectrum sum of the most abundant CR species (p, He, C, O and Fe). The vertical dashed line at 10^{15} eV marks the maximum energy (10^{15}) eV that can be measured by a CR detector in orbit [2].

2.1 Electro Magnetic Showers

As mentioned, there are several types of particles that are the cause of extensive air showers. The first of which being high-energy electrons, or beta particles and the second being a high-energy photon. These two in particular are the instigator for a so called electromagnetic shower. While there various processes involved for these particles such as Compton scattering and the photo-electric effect, the ones of significance for this project are `Pair Production` and `Bremsstrahlung` for photons and electron-positron pairs.
Bremsstrahlung is process by which a high energy electron emits a photon when interacting with the electromagnetic field of a nucleus. Pair production is the process that occurs when the photon interacts with the Coulomb field of the nucleus causing it to disappear. As result of this interaction a electron-positron pair is created [3].
Through these processes the high-energy primary particle will produce secondary particles, which in turn produce new particles with a lower energy creating an electromagnetic shower.

2.1.1 Heitler's Toy Model

To simplify the complex evolution of extensive air shower development W. Heitler proposed his toy model for electromagnetic cascade development [4] and can be seen in figure 2. This model has e^-, e^+ and photons undergo continual two-body splotting, one-photon bremsstrahlung or e^-e^+ pair production. In addition the model follows a set of simplified assumptions:

- The shower development is assumed to be a uniform process rather than the intrinsic random development process that takes place in the corporeal world.
- The shower development halts once the critial energy threshold has been reached, while in reality this process is approached in a smoother fashion.
- The photon, electron and positron are assumed to have the same radiation length, X_0, causing it to split at a fixed distance.
- Once a particle has traveled exactly a certain length, half of its energy will have been lost by producing a daughter particle which inherits half of the initial energy.

To represent the number of radiation lengths a dimensionless variable n is introduced:

$$n = \frac{X}{X_0} \tag{1}$$

After n radiation lengths there will be 2^n secondary particles each with an energy of $E_0 \cdot 2^{-n}$, where E_0 represents the energy of the primary particle. The shower development will halt once the secondary particles with energy E_n reach the critical energy E_c^{em}, where the energies of the particles are too low for both pair production and bremsstrahlung.

$$E_n = \frac{E_0}{2^n} = E_c^{em} \tag{2}$$

The value for the critical energy will be dependent on the medium in which the shower has developed. Thus, at the depth of $E_n = E_c^{em}$, the cascade has reached the maximum number of secondary particles. By using the previous equation one can determine the the maximum number of radiation lengths:

$$n_{max} = \frac{ln(E_0/E_c^{em})}{ln(2)} \tag{3}$$

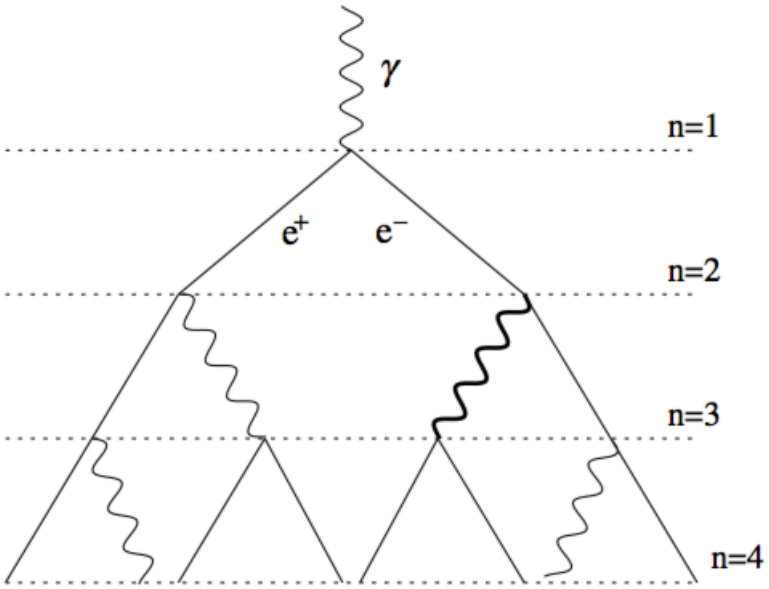

Figure 2: Heitler Toy Model for electromagnetic showers. The straight lines represent either a positron or electron, while the wave line represents a photon. [5]

with the corresponding maximum number of particles:

$$N_{max}^{em,\gamma} = \frac{E_0}{E_c^{em}} \tag{4}$$

where the superscript γ denotes the inclusion of photon induced secondary particles [6].
Lastly the depth at which the air shower reaches the maximum number of particles can be expressed as:

$$X_{max} = X_0 \frac{log(\frac{E_0}{E_c})}{log2} \tag{5}$$

and is measured in $g\,cm^{-2}$. While the toy model does not capturing the finer details of EM showers two features are accounted for. First is the total final number of photons, electrons and positrons, N_{max} is proportional to the initial energy of the primary particle, E_0. Secondly the depth of maximum shower development is proportional to the logarithm of E_0 [4].

2.2 Hadronic Showers

In comparison to the electromagnetic counterpart, the hadronic component of an extensive air shower has a more complex development. In addition to photons, electrons and positrons that are present in the electromagnetic shower there is the muonic component, which includes muons and neutrinos, and the hadronic component, containing pions, kaons and baryons. A representation of the distinction between these components can be viewed in Figure 3.
Following the initial interaction of the primary particle, nucleons or baryons, with the atmosphere a diverse set of different particles is created through both strong and electromagnetic interactions. To deal with the complexity of hadronic showers a model similar to Heitler's toy model has been created. After the initial collision an equal number of pions with different charge, π^0, π^+, π^-, are created. The neutral pion, π^0 has a lifetime of $\tau = 10^{-16}$ s and decays into two photons [6] causing the creation

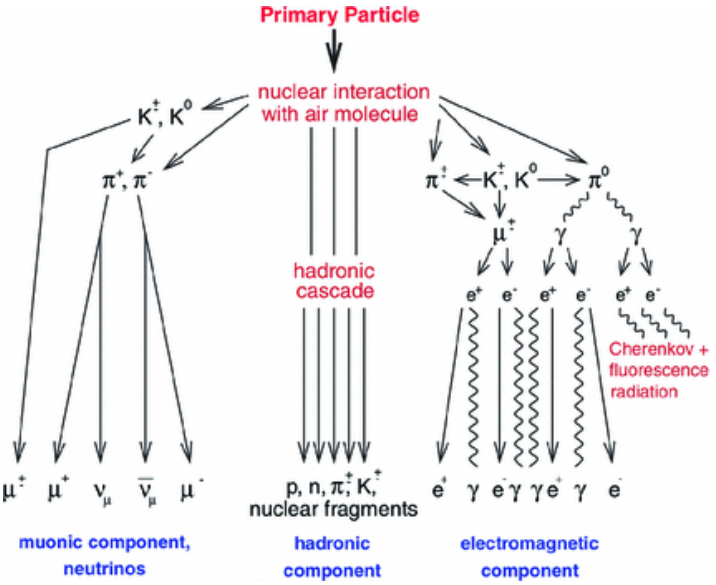

Figure 3: Scheme of an EAS. The secondary particles are grouped into three components with, from left to right, the muonic component including neutrinos, the hadronic component and the electromagnetic component [7].

of two electromagnetic subshowers. The charged pions, with a lifetime of $\tau = 10^{-8}$ s [6], travel a set distance and through interaction create a new generation of pions. Similar to the EM cascade, the hadronic component will continue with this multiplication process until individual pions drop below a certain critical energy, E_c^{π}, from which onwards the charged pions, $\pi^{\pm}$, are assumed decay into muons or neutrinos [8]. A simplified visualization of this process can be found in Figure 4.

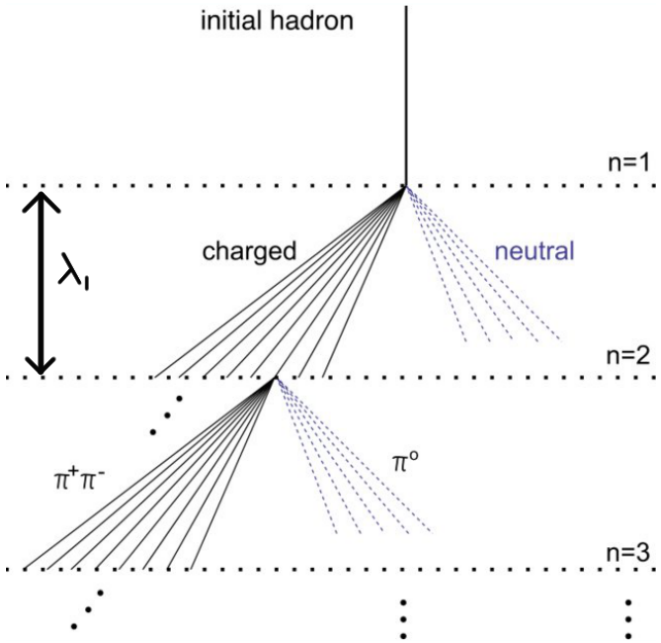

Figure 4: Heitler-Matthews Model for hadron showers [9]. First three steps of a hadronic cascade with the with the solid lines representing charged particles and the dashed line indicating neutral particles. From the second step only a single splitting is portrayed. λ_I signifies one interaction length of strongly interacting particles.

At each step in the hadronic component various hadronic daughter cascades are produced. This number of reaction products is know as the particle multiplicity of the reaction, denoted by n_m. The charged to neutral ratio for pions has a value of $r \simeq 2/3$, similarly the C/N ratio for kaons and nucleons is 1.5 and 1 respectively [3]. Thus the total number of charged pions at generation n within a hadronic cascade is

$$N_n^{ch} = (r\, n_m)^n \tag{6}$$

with the energy per pion at

$$E_n^{\pi} = \frac{E_0}{(n_m)^n} \tag{7}$$

which gives a familiar form to that of the EM shower component. However, due to the multiplicity of the hadronic component being larger than its EM counterpart the energy of the secondary particles will lessen at a more rapid pace for each generation. The number of generations, n_c, needed for E_n^{π} to reach the critial energy, E_c^{π}, can be expressed in the following way

$$n_c = \frac{ln[E_0/E_c^{\pi}]}{ln[n_m]} \tag{8}$$

which can be further simplified to $0.85\, log_{10}[E_0/E_c^{\pi}]$ when assuming $r \simeq 2/3$.
Due to the energy diminishing for each generation n the decay length decreases in accordance with E_n^{π} resulting in

$$l_{decay} = \frac{E_n^{\pi}}{m_0 c^2} c\tau \tag{9}$$

where $m_0 c^2$ signifies the rest energy of the pion and τ the lifetime in seconds [6]. Once this decay length has fallen below the interaction length, λ_I, no new pions will be created. Rather, at this depth a charged pion will instead decay into a muon or neutrino thus marking the endpoint of the shower development.
As a consequence of the diminishing energy of each generation changing at a different rate for the hadronic and electromagnetic components one is forced to review the depth at which the maximum number of particles is achieved seperately. For both muons and pions this depth is the same and estimated by:

$$X_{max}^{\mu} \approx X_{max}^{\pi} = \lambda_I \; ln\,(E_0/E_c^{\pi})\, \frac{1}{ln(n_m)} \tag{10}$$

For the electromagnetic component of a hadronic shower the depth at which the maximum number of particles achieved is estimated by:

$$X_{max}^{em} = \lambda_I + X_0\, ln\left(\frac{E_0}{2 n_m E_c^{em}}\right) \tag{11}$$

Where the interaction length, λ_I, takes into account that the first photons will only be created after the first collision.

2.3 Detection Techniques

Depending on their energy, cosmic rays can be measured directly by balloon and satellite experiments, up to about 10^{15} eV. Above this energy, the flux is too small, and the cosmic rays are measured indirectly on the ground by sampling the showers they generate hitting the Earth's atmosphere.
Several types of detectors can be employed to perform ground-based detection of cosmic rays.
Air shower arrays consist of particle detectors located at different distances from each other, from a few to several hundred meters, depending on the energy of the primary detected particles. These detectors can be used to study a wide energy range, from 10^{15} eV upwards. For example, in the Pierre Auger Observatory, which aims at detecting the highest cosmic rays of energy above 10^{19} eV, the distance between two detectors is 1500 m.
Imaging Atmospheric Cerenkov Telescopes (IACTs) detect the Cerenkov light emitted by the shower-charged particles (mainly electrons and positrons) in the atmosphere. Most of the light comes from the shower maximum. These detectors target the energy range between about 10 GeV and hundren TeV.
Fluorescent detectors detect the fluorescent light from the Nitrogen atoms in the atmosphere that are excited by the ionisation of the shower-charged particles. Unlike the Cerenkov light, fluorescent light is isotropic and can be observed over a significant distance of several tens of km. This technique can be effectively used only for the highest energy particles, above about 10^{19} eV.

3 Methodology

Throughout this project two kinds of functions will be tested, with the aim to determine which of the two functions better describes a variety of shower profiles. The majority of the processing, fitting and visualizing of the data has been accomplished using the ROOT framework.

3.1 ROOT

The ROOT [10] analysis framework, developed by CERN, is an object orientated framework used in the field of particle physics to process, analyze, and fit data. In addition, due to the capability to process large amounts of data, ROOT is used to perform large scale simulations within the field of High Energy Particle Physics. The framework uses a build-in C++ interpreter Cling which utilizes the Low Level Virtual Machine (LLVM) [11] as its compiler infrastructure acting in collaboration with the Clang Libraries [12] as a front end compiler for the C and C++ programming languages.

3.2 Modules and Classes

In this section brief descriptions will be given of various modules and classes native to the ROOT system. When one of these is utilized throughout the data processing there will be a more detailed explanation given.

TFile The ROOT system works with a data structure called `.root` files containing consecutive data records. ROOT files contain objects and directories and is designed in such a way that one can write in pure sequential mode.

TBrowser This class displays all browsable ROOT classes from the selected `.root` file and allows one to view all browsable objects in either a new list or window.

TTree In the ROOT system data is stored within a `TTree` as a columnar dataset capable of storing any C++ type up to 1 EB (10^3GB) of data. These lists of independent columns are also called branches which with the help of automatically allocated buffers allow the data to be kept in memory allowing select branches to be called upon when not all the data is needed, thus speeding up analysis process.

TChain The `TChain` module is used to chain together a collection of `TTree` datasets from different `.root` files. Once a chain is defined the branches of these TTrees can then be activated to be used as one sees fit.

TH1 `TH1` is the base class for all histogram types in ROOT. This includes operations such as binning, filling, drawing and fitting for 1-D, 2-D and 3-D type histograms. In particular there will be made use of type `TH1D` and type `TH2D`, both utilizing one double per channel for maximum precision of 14 digits.

TF1 The `TF1` is the 1-Dimensional constructor which allows an object to be fitted to a 1-D function between a lower and upper limit. This function can be either a general C++ function or a precompiled user function, with or without parameters. This function can then be drawn with the `TH1` class or dedicated `TGraph` class.

TRandom This is the base class for the Random Number Generators available in ROOT. The generator itself is a Linear Congruential Generator (LCG) which determines the randomized numbers through a discontinuous piecewise linear equation. The sequence of random distributed numbers can be determined through several kinds of distributions; such as a Gaussian distribution or Poisson distribution. For this project however it has been decided to instead use a uniform distribution on a chosen interval.

3.3 CONEX data

The Data used in this project has been simulated[1] with the program `CONEX` [13, 14] using the high energy hadronic interaction model `QGSJETII-04` [15] to generate 1-Dimensional simulations of Extensive Air Showers, including fluctuations. `CONEX` is a hybrid simulation code that combines explicit Monte Carlo simulations of the cascade for high energy particles together with a numerical solution of nuclear-electro-magnetic cascade equations resulting in distributions of secondary particles [13]. In this simulation one follows the propagation, interactions and decay of nucleons, charged pions, and both charged and neutral kaons. Even though other hadronic particles are produced through interactions and decays, they are assumed to decay immediately.
The simulated showers for this project several primary particles, (γ, proton and iron), have been selected each at various energies. Both the Zenith and Azimuth angle have been fixed to 0 degrees for all simulations. For High Energy interactions the `QGSJETII-04` model has been selected and for the Low Energy model `UrQMD` [16] has been selected, with a transition energy from low to high hadronic interaction model set at 80 [GeV]. For each primary with correlating energy a set of 1000 showers, or events, has been simulated.

3.4 The shower profile

Starting off, after importing the data set and setting the branches for use it was decided to plot the shower development of the several particles. This includes Hadrons, Muons, positively and negatively charged Electrons, and a summation of these under Charged Particles. This check was performed with the `TGraph` class and was plotted as a function of slant depth $X\,[g/cm^2]$ and was tested on several events. The aim of this was to see if the simulated showers were properly imported before further results were obtained. A plot of one of these events can be seen in figure 5. This event is taken from the data set with an Iron nucleus as the primary particle and an energy fixed at 100 [TeV]. Similar events with different primary particles, γ and proton, can be found in the appendix under figure 23 and figure 24. In addition, as preparation for the fitting procedure of several functions at a later stage, a simple second degree polynomial was fitted around the maximum of the profile of the charged particles.
Using the second degree polynomial one has the ability to make a first guess of the for the maximum number of particles in the shower, N_{max} and the longitudinal depth at which the shower reaches the maximum number of particles, X_{max}. Using the class `TF1` to fit the second degree polynomial over a select range, 200 $[g/cm^2]$, around the maximum data point one is able to make the first reliable guess for the parameters N_{max} and X_{max} for all simulated events. Having attained these values and making use out of the `TH1D` class, a 1-D distribution of X_{max} for the Iron primary at 10 TeV can be plotted and is visible in Figure 6.

[1] The simulated events were provided by Andres G. Delgado Giler and stored in the Kapteyn cluster

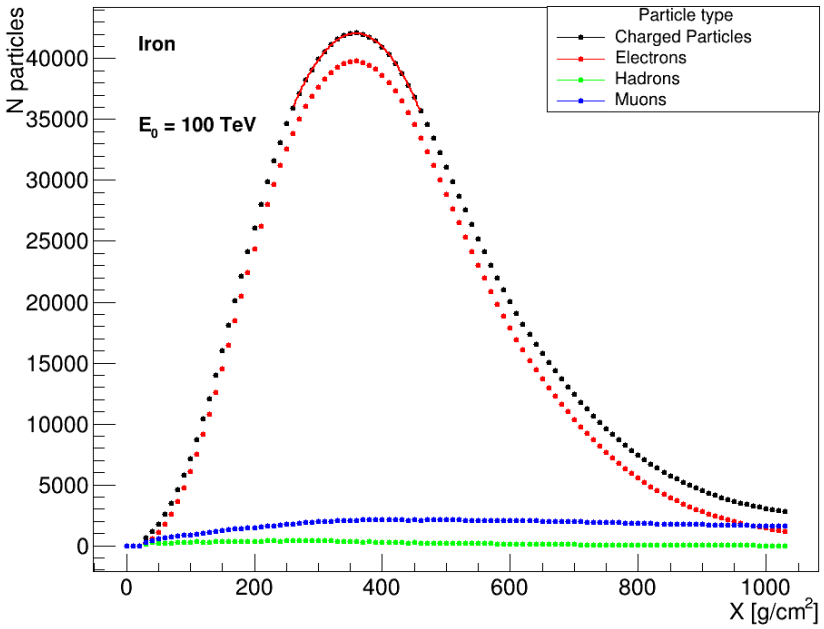

Figure 5: Shower development of a single event with Iron primary at 100 TeV. The black dots indicate the sum of all the other components, namely electrons (including positrons), charged hadrons and muons

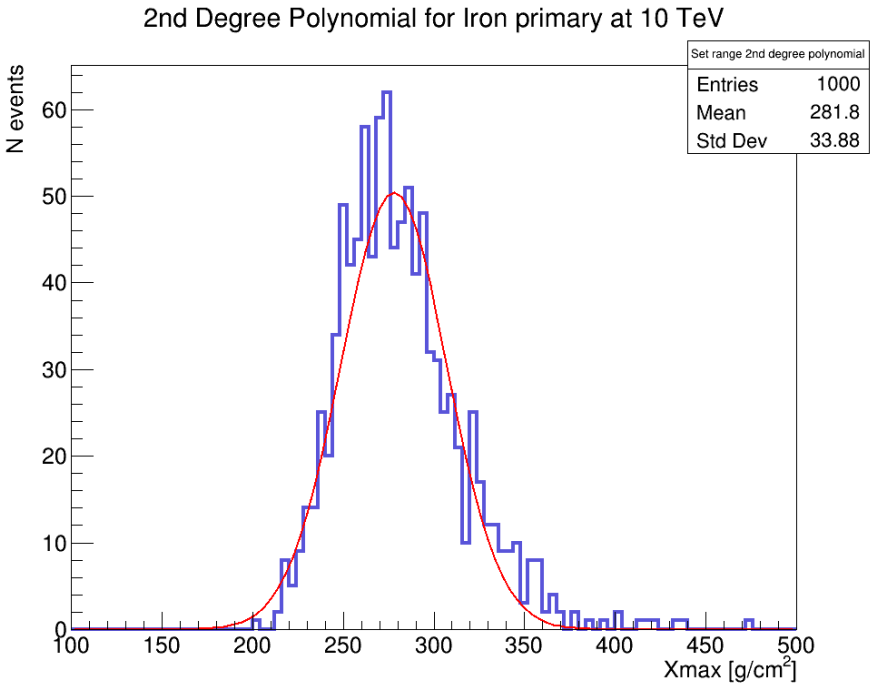

Figure 6: Distribution of X_{max} obtained through fitting a second degree polynomial of the simulated showers generated by primary cosmic-ray iron with 10 TeV energy. The mean value and standard deviation seen in the top right are obtained through a normal distribution fit to the data and is signified in red.

3.5 Characterization of the shower maximum over the whole atmospheric depth range

The number of charged particles of an extensive air shower can be parameterized by potentially two different functions. Each of them will briefly be discussed in the following section.

The Gaisser-Hillas function was first proposed by Thomas K. Gaisser and Anthony Michael Hillas as a method to parameterize the longitudinal particle density in a extensive air shower [17] [18]. The number of particles, $N(X)_{GH}$, is expressed as a function of transverse atmospheric depth, X, and reads as follows:

$$N(X)_{GH} = N_{max}\left(\frac{X - X_0}{X_{max} - X_0}\right)^{\frac{X_{max}-X_0}{\lambda}} e^{-\frac{X-X_{max}}{\lambda}} \tag{12}$$

Here N_{max} represents the number of particles at the depth of the shower maximum X_{max}, X_0 represents the starting depth in the atmosphere and is usually a negative free parameter, and λ is the attenuation length of the particles. It does have to be mentioned that both X_0 and λ have no physical meaning.

The Gaussian In Age function [19], rather than being expressed in depth, X, the longitudinal development is expressed as a function of shower age, s, and is as follows:

$$s = \frac{3X}{X + 2X_{max}} \tag{13}$$

Through this method the shower longitudinal development is described as a rising phase from 0, the initial position of the shower, to 1, the shower maximum. Then for a physical shower there will be a decay phase between $s = 1$ and $s = 2$. The shower age parameter is subsequently implemented in the adjusted Gaussian function.

$$N(s)_{GIA} = N_{max}\, e^{-\frac{1}{2}\left(\frac{-1}{\sigma}\right)^2} \tag{14}$$

Both the Gaisser-Hillas and Gaussian in Age method will be fitted on the full range of the shower profile. An example of one of these events for an Iron primary particle with an energy of 10 TeV can be seen in Figure 7.

The starting parameters for the Gaisser-Hillas function we pick an initial value of -120 for X_0, to signify the starting point of the primary particle to be above the first collision. A value of 90 for λ, and filling in the first guess parameters obtained from the second degree polynomial, N_{max} and X_{max}, into their respective parameters in the GH function to obtain X_{max}^{GH} for all events. Calling upon the `Fill` function from class `TH1` a 1-D distribution can be plotted resulting in the plot seen below in figure 8. The X_{max}^{GIA} parameter for the Gaussian In Age function is obtained through similar methods as the GH function. The 1-D distribution of parameter X_{max}^{GIA} can be seen in figure 9.

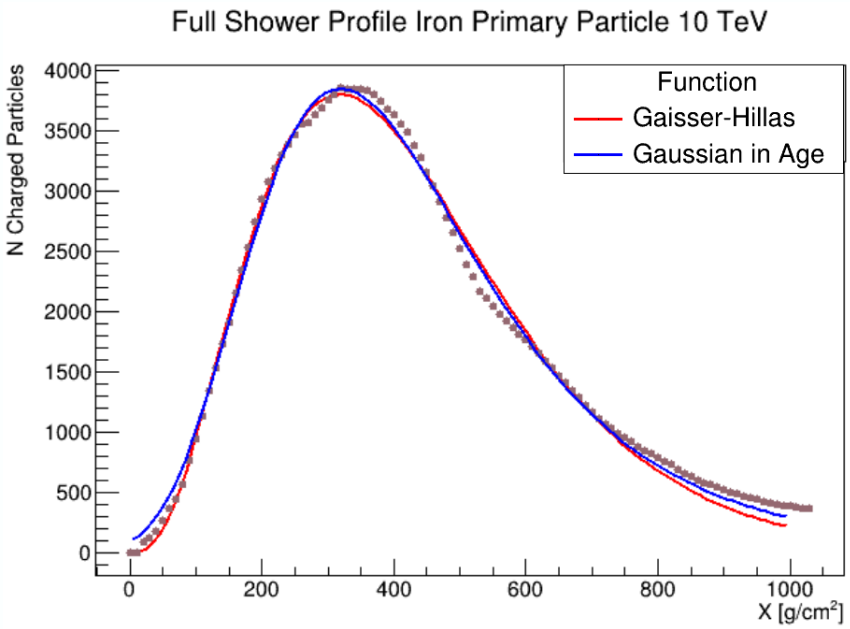

Figure 7: Shower profile for simulated iron events with 10 TeV energy (brown dots), fitted to the Gaisser-Hillas function (red curve) and to the Gaussian in Age function (blue curve).

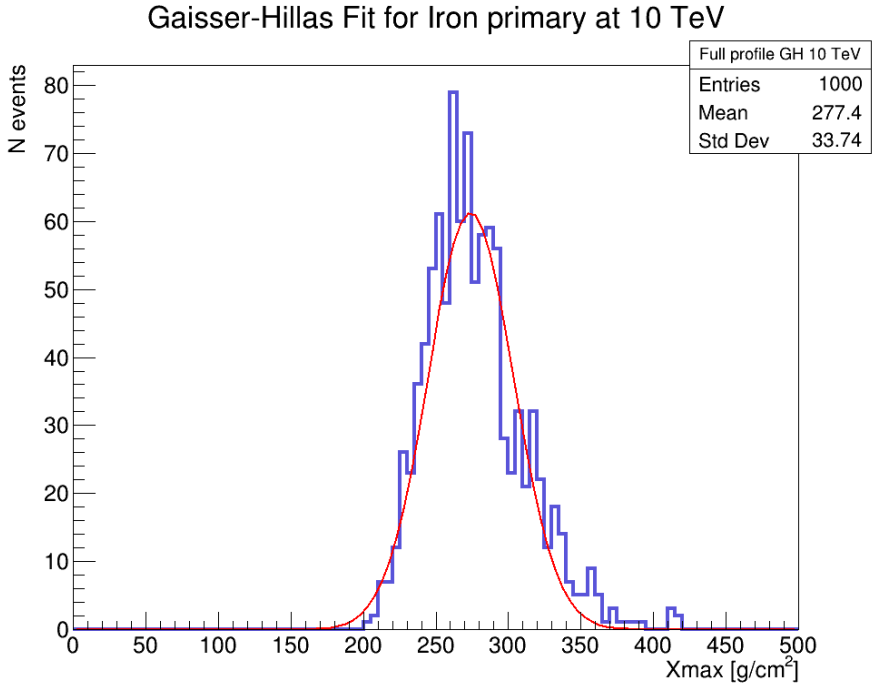

Figure 8: 1 dimensional distribution of X_{max} obtained through the fit of the Gaisser-Hillas function on primary Iron at 10 TeV. The mean value and standard deviation seen in the top right are obtained through a normal distribution fitted over the data and is shown in red.

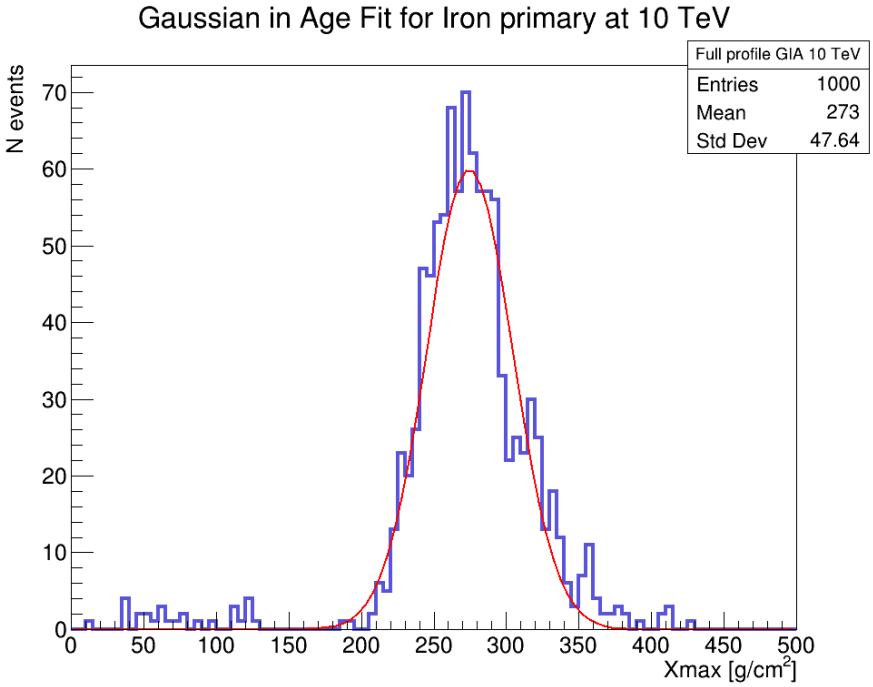

Figure 9: 1 dimensional distribution of X_{max} obtained through the fit of the Gaussian in Age function on primary Iron at 10 TeV. The mean value and standard deviation seen in the top right are obtained through a normal distribution fitted over the data and is shown in red.

The distribution of the difference between X_{max}^{GH} and X_{max}^{GIA} found between the two functions for one thousand iron primary events can be seen in figure 10. Plotting these distributions and extracting the mean through `TF1::GetMean` allows one to compare the reliability of the two fitting methods to each other. The implication is that the the closer the Mean value is to 0, the more the two fitting methods agree with each other. This will be further explored and discussed in the Results section. The histogram for the remaining primary energy of Iron can be found in the appendix at figure 25 to figure 27.

3.6 Characterization of the shower maximum using a limited atmospheric depth range

To determine which fitting method is more reliable when the full profile is unavailable there will be analysis with constraints in place regarding the range in which the two functions can be fitted around the previously guessed maximum position. To achieve this restricted range will vary for each event through the use of a random number generator. This is done with a Linear Congruential Generator [20] build within ROOT's interface. It's constructor, `TRandom`, has like mentioned earlier several methods to generate random numbers according to several distribution processes. Since a single integer generated for each event suffices `TRandom::Integer` has been used. Through this method a random integer which is uniformly distributed on an earlier decided interval [0, 100] will be selected. The left boundary and right boundary are decided by separate randomly generated values to avoid symmetry within the fit. However, because of this there could occur a scenario where the left boundary gets assigned a value of 100 while the right boundary gets assigned a value of 0, creating a skewed distribution. To prevent this from occurring a value of 50 will always be added to the value generated from the interval for both the left and right boundary. This results in a total restricted range

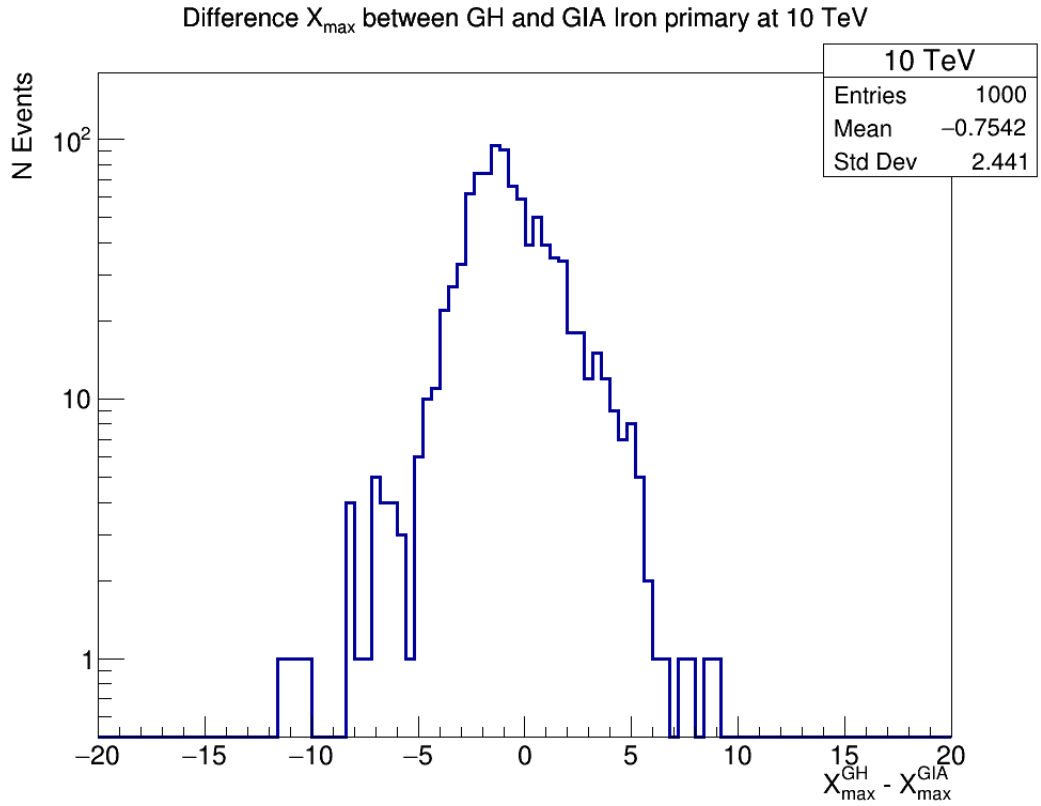

Figure 10: 1-D distribution of the difference for the position of X_{max} between the Gaisser-Hillas function and the Gaussian in Age function when fitted over the full shower profile of the iron primary particles at 10 TeV.

between 100 g/cm^2, when both values are generated to be 0, and 300 g/cm^2, when both boundaries get assigned a value of 100. Several plots of the same event with randomly assigned ranges and fits can be found in figure 11. Fitting the shower profile to this range for both the Gaisser-Hillas function and Gaussian in Age function yields X^{*GH}_{max} and X^{*GIA}_{max} respectively.
Having acquired the maximum longitudinal depth, X^{*}_{max}, for both functions fitted on these cut-profiles, one can obtain:

$$\Delta X^{cut\,GH}_{max} = X^{GH}_{max} - X^{*GH}_{max} \tag{15}$$

and

$$\Delta X^{cut\,GIA}_{max} = X^{GIA}_{max} - X^{*GIA}_{max} \tag{16}$$

Where ΔX^{cut}_{max} is the difference between the maximum longitudinal depth obtained before and after the fitting range got restrained. With the `TH1` class a histogram will be plotted for both distributions for each primary particle and energy. From this distribution one can, by means of a Normal distribution, extract both the Mean value and Standard Deviation which in turn will be plotted as a function of energy for analysis later.

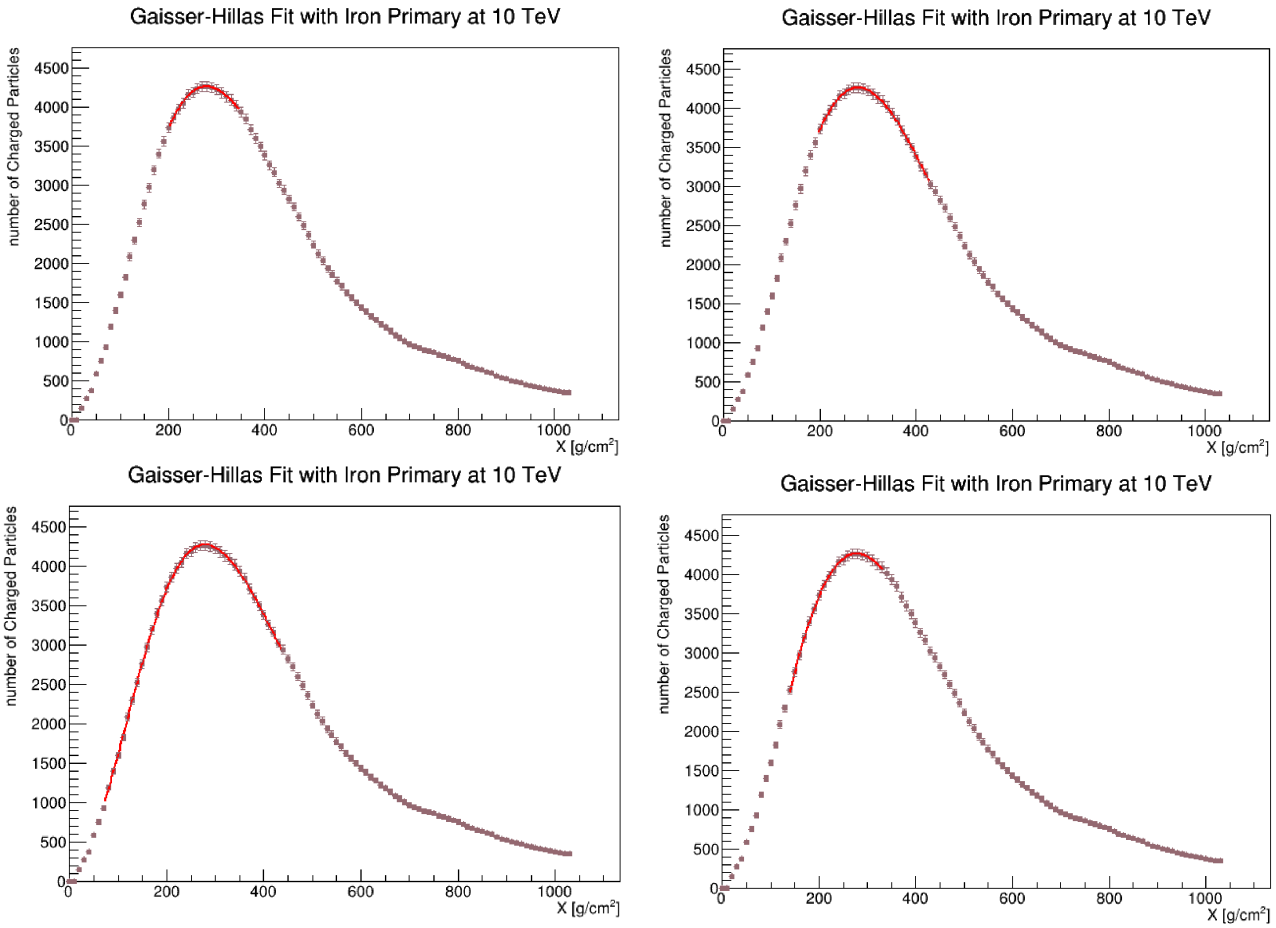

Figure 11: Same Iron event with an energy of 10 TeV fitted with Gaisser-Hillas function on randomly selected ranges.

4 Results: Presentation

The first segment of the results will devoted to solely to the display of what has been accomplished and an explanation of what can be seen on the multitude of distributions, Graphs, and Fittings

4.1 Full Profile Fittings

Figure 12 and Figure 13 show the 1-D distributions of X_{max} fitted with the Gaisser-Hillas method and the Gaussian In Age method respectively when the full shower profile has been included. Both of these figures have an Iron nucleus as their primary particle and include all energies (10 TeV, 50 TeV, 100 TeV, 300 TeV). The horizontal axis displays at which position an event has reached would have reached the maximum number of particles achievable, while the vertical axis shows how many of the events have that maximum position as their peak.

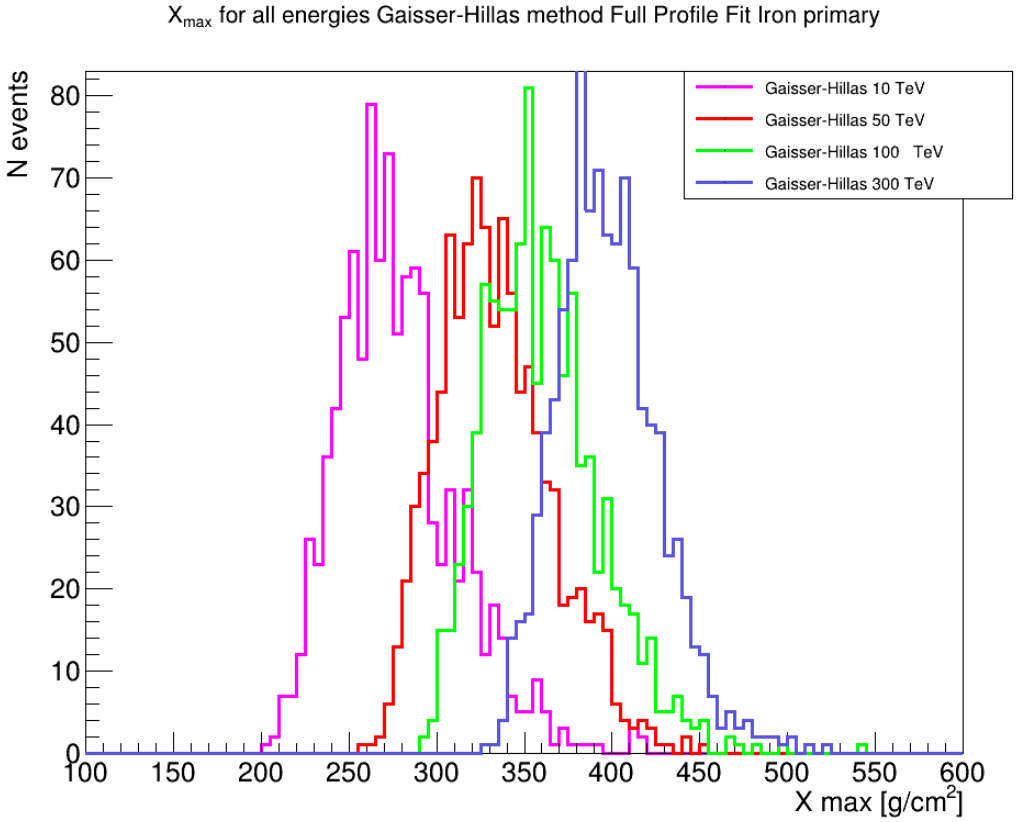

Figure 12: Histograms of the 1-D distribution of maximum longitudinal depth, X_{max}, for the Iron Primary particle using multiple energies fitted using the Gaisser-Hillas function on the entire shower profile.

The distributions and histograms for the γ primary particle for both the GH function and GIA function can be found in the appendix under figure 26 to figure 27. It has to be mentioned that unlike the Iron and Photon primary particle, that the different energies for the Proton primary particle fitted on the full shower profile have been left out. The reasoning for this the amount of overlap each energy would have with the others, rendering the plot useless. Furthermore the exact values of X_{max} for the Iron primary particle at each energy can be seen in Table 1 below. In addition the exact values for the

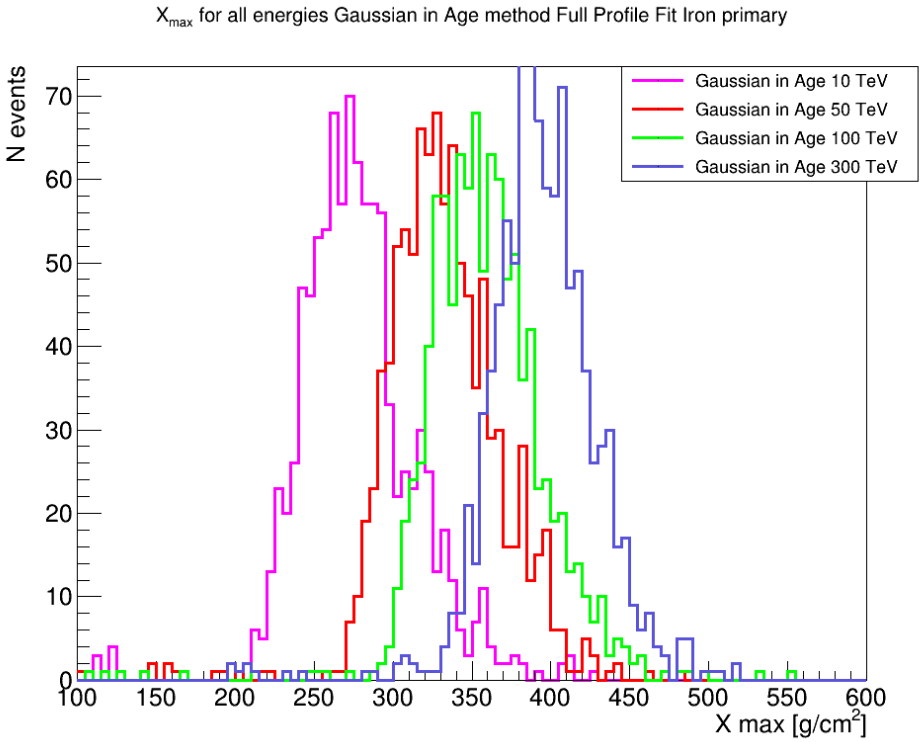

Figure 13: Histogram of the 1-D distribution of maximum longitudinal depth, X_{max}, for the Iron Primary particle using multiple energies fitted using the Gaussian In Age function on the entire shower profile.

Proton and Photon can be found in the appendix under Table 3 and Table 4. Looking at these values one is able to verify the correlation between the energy of the primary particle and X_{max}.

X_{max} Values Iron Primary Particle Full Shower Profile		
Energy	Gaisser-Hillas	Gaussian In Age
10 TeV	277.421 ± 1.06681	277.17 ± 1.18886
50 TeV	333.313 ± 1.00707	331.671 ± 1.1818
100 TeV	360.035 ± 1.03329	358.618 ± 1.2009
300 TeV	397.737 ± 0.920638	394.954 ± 1.11201

Table 1: The values for longitudinal depth at the maximum number of particles, X_{max}, for an Iron Primary Particle with different energies. Fitted with both the Gaisser-Hillas model and the Gaussian In Age model applied to the Full Shower Profile.

Figure 14 shows the average difference the two fitting methods, GH and GIA, have regarding their agreement on the maximum longitudinal depth, X_{max}, for the Iron primary, Photon primary and Proton primary when applied to the full shower profile. On the horizontal axis of represents the energy of each particle in TeV. The vertical axis represents the Mean value of the distribution of the difference of X_{max} between the two fitting methods. The closer this value is to zero the more both fitting method agree with each other. The exact values can be viewed in Table 2 of the discussion section.

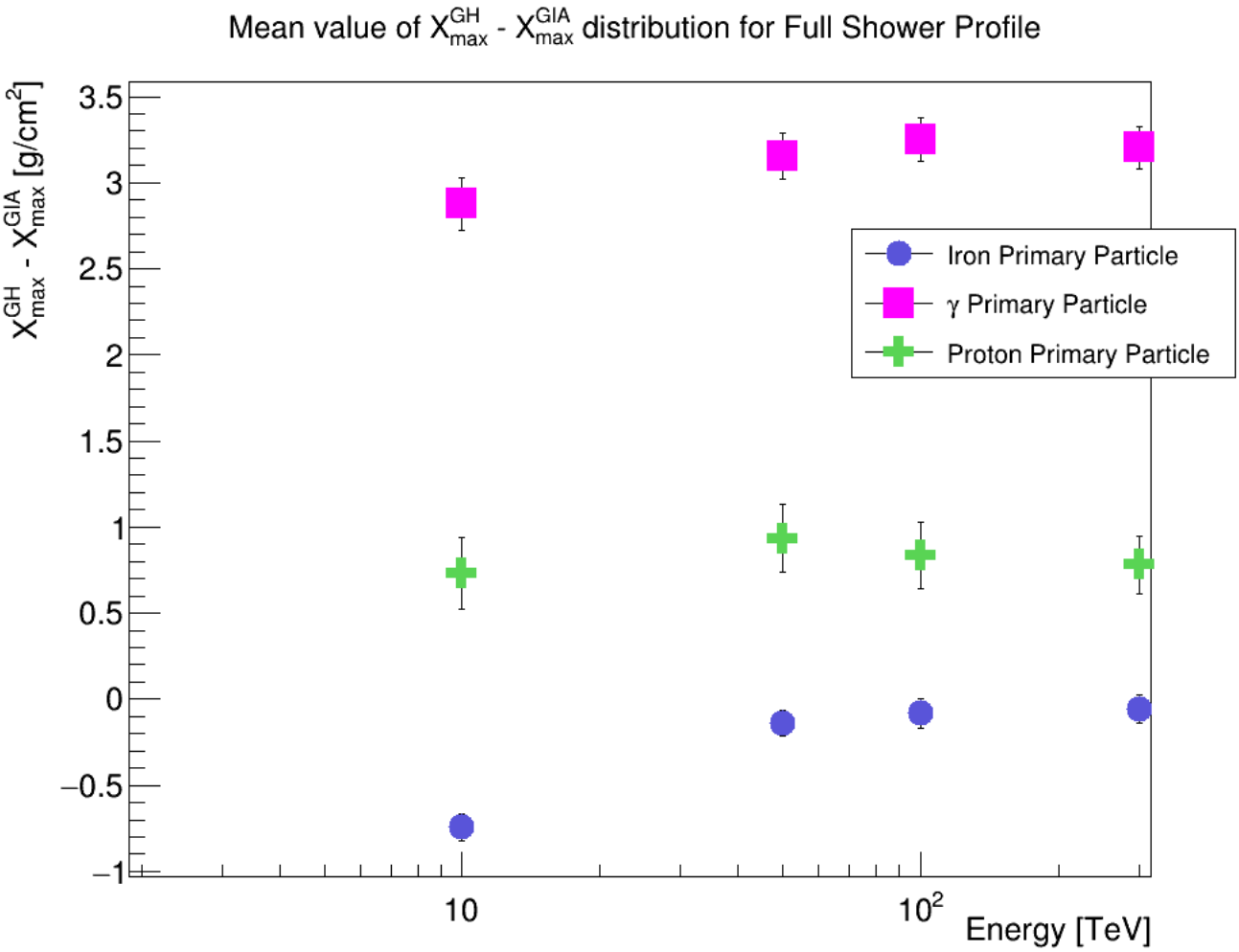

Figure 14: 1-D plot describing the Mean value of the difference between the Gaisser-Hillas and Gaussian In Age function when fit to the Full Shower Profile.

4.2 Cut Profile Fitting

Figure 15 and Figure 16 show the 1-D distribution of X^*_{max} at 10 TeV for both the Gaisser-Hillas and Gaussian In Age functions when fitted on a restricted range profile. Likewise the remaining energies of the Iron primary particle and all energies of the γ and Proton primary particles are in the appendix from figure 28 to figure 37. Similar to Figure 12 and Figure 13 the horizontal axis represents the position where the maximum number of secondary particles is achieved and the vertical axis represents the number of events. In addition, a Normal distribution, in red, has been fitted on each plot to attain the Mean value and Standard Deviation of their respective distribution. These values represent at which position the maximum number of secondary particles , X^*_{max}, will be achieved.

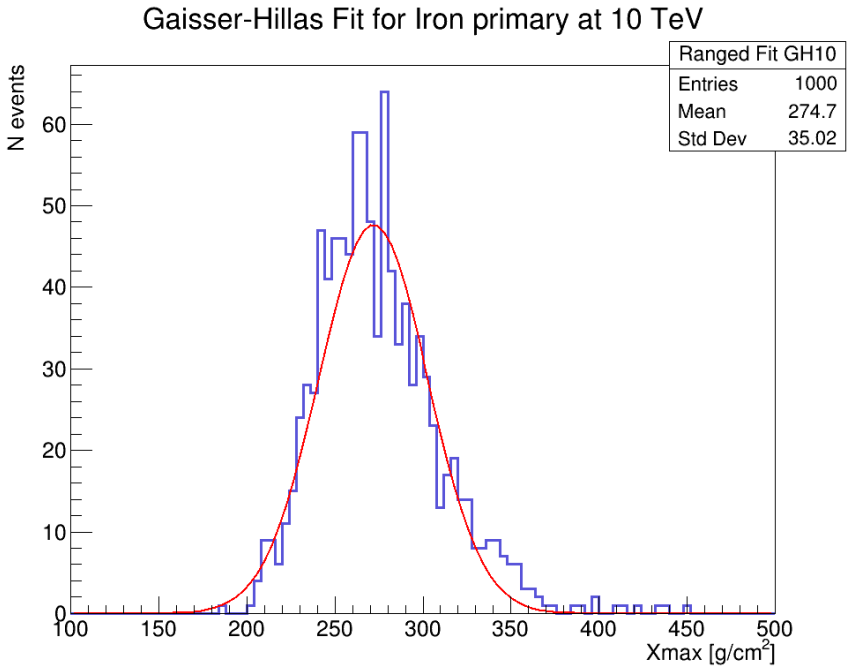

Figure 15: Histogram of the 1-D distribution of maximum longitudinal depth determined, X^*_{max} by the Gaisser-Hillas function for the Iron Primary Particle at 10 TeV when fitted to a restricted range of the shower profile.

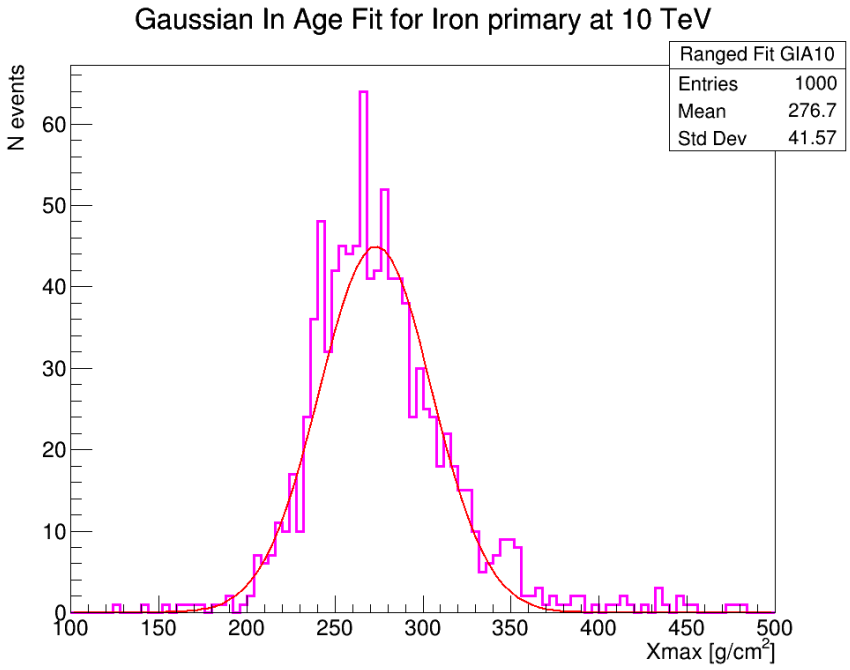

Figure 16: Histogram of the 1-D distribution of maximum longitudinal depth determined, X^*_{max} by the Gaussian In Age function for the Iron Primary Particle at 10 TeV when fitted to a restricted range of the shower profile.

Figure 17 displays the histograms of the difference between the maximum position of the full profile fit, X_{max}, and the restricted profile fit, X^*_{max}. This value is also referred to as ΔX^{cut}_{max}. Figure 17 includes

both methods, GH and GIA, for the Iron primary particle at 10 TeV. Both also have had a Normal distribution fitted to their data, which is displayed in red. Similar to previous plots, the vertical axis represents the number of events. The horizontal axis represents the difference of maximum position between the full and restricted shower profile fit in units of g/cm^2. The appendix contains the remainder of the different energies and primary particles from figure 38 to figure 48.

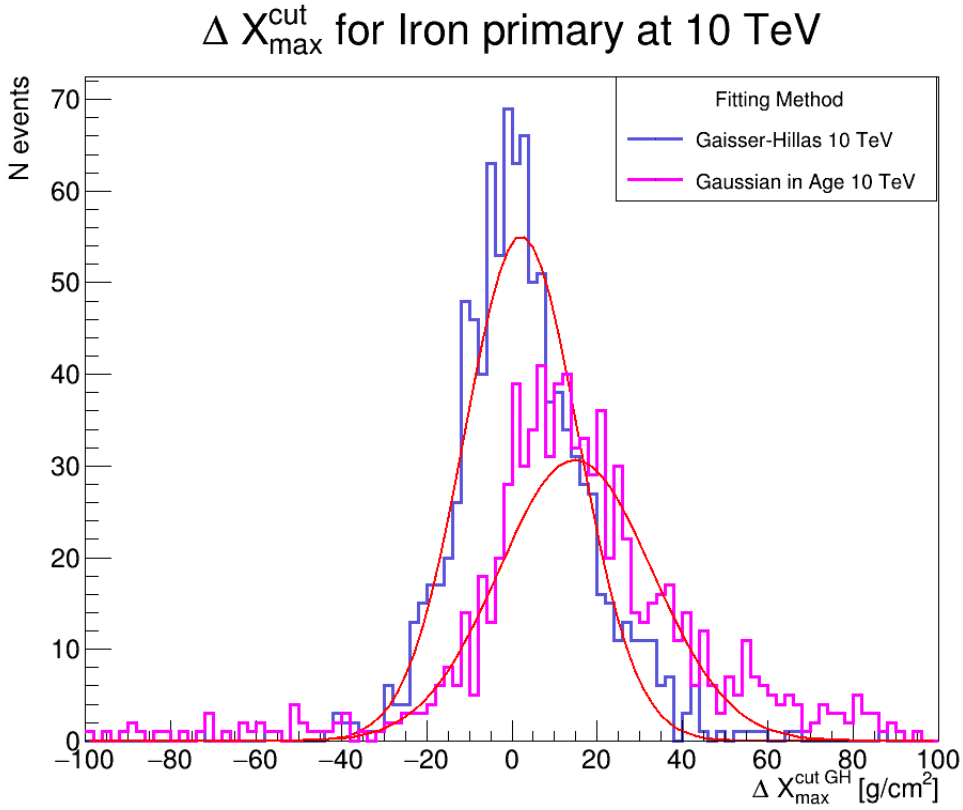

Figure 17: Histogram of the 1-D distribution of ΔX_{max}^{cut} for both the Gaisser-Hillas and Gaussian In Age function for the Iron Primary Particle at 10 TeV.

Figure 18 presents the previously mentioned Mean values of the ΔX_{max}^{cut} distribution for both fitting methods on the Iron primary particle. On the vertical axis, displayed one can see the value representing the difference between full profile fit and ranged profile fit in units of g/cm^2. On the horizontal axis, in logarithmic scale, the energy in TeV is displayed. As the Mean value of ΔX_{max}^{cut} approaches zero, the more the full profile fit and cut range fit agree with each other showing a lesser sensitivity to the choice of fit range. The figures relating the Mean from the γ and Proton primary can be found in in Figure 49 and Figure 50 in the appendix.

Figure 19 contains the Standard Deviation from the ΔX_{max}^{cut} distribution of the Iron primary particle for both the GH and GIA fitting method plotted as a function of energy. Similar to figure 11 it displays the energy in TeV on logarithmic scale on the horizontal axis. The vertical axis represents the Standard Deviation in g/cm^2. As the Standard Deviation approaches zero it implies a stronger certainty in the Mean value. The figures for the remaining particles can be found in the appendix under Figure 51 and 52 .

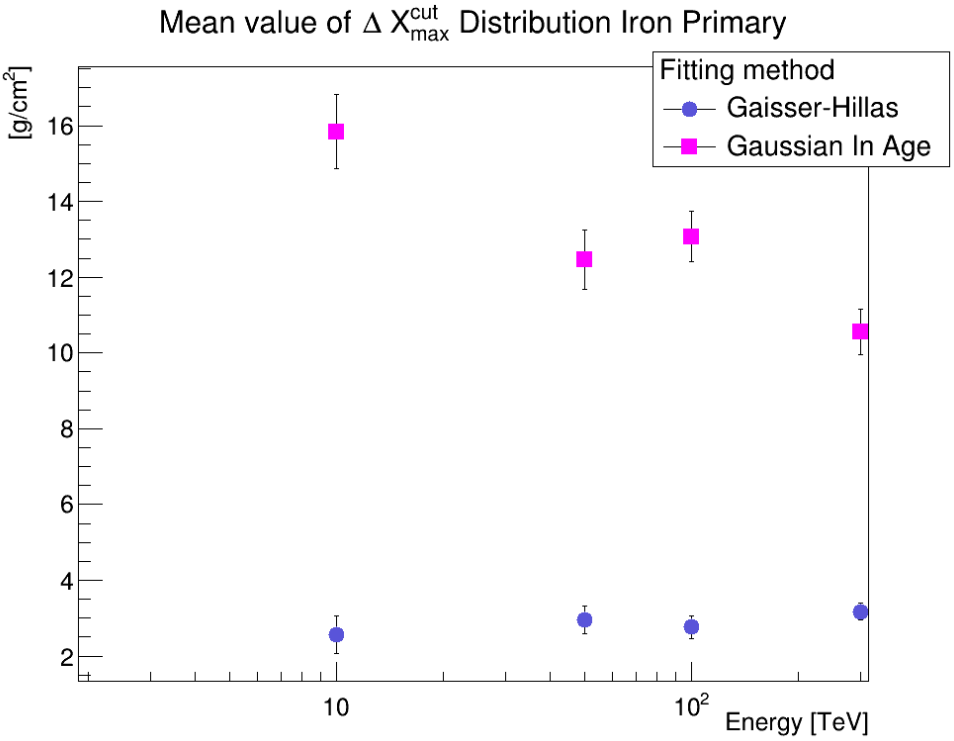

Figure 18: The mean value of the difference between the full profile, X_{max}, and the cut profile, X^*_{max}, for both the Gaisser-Hillas and Gaussian in Age function when fitted on the iron primary particle.

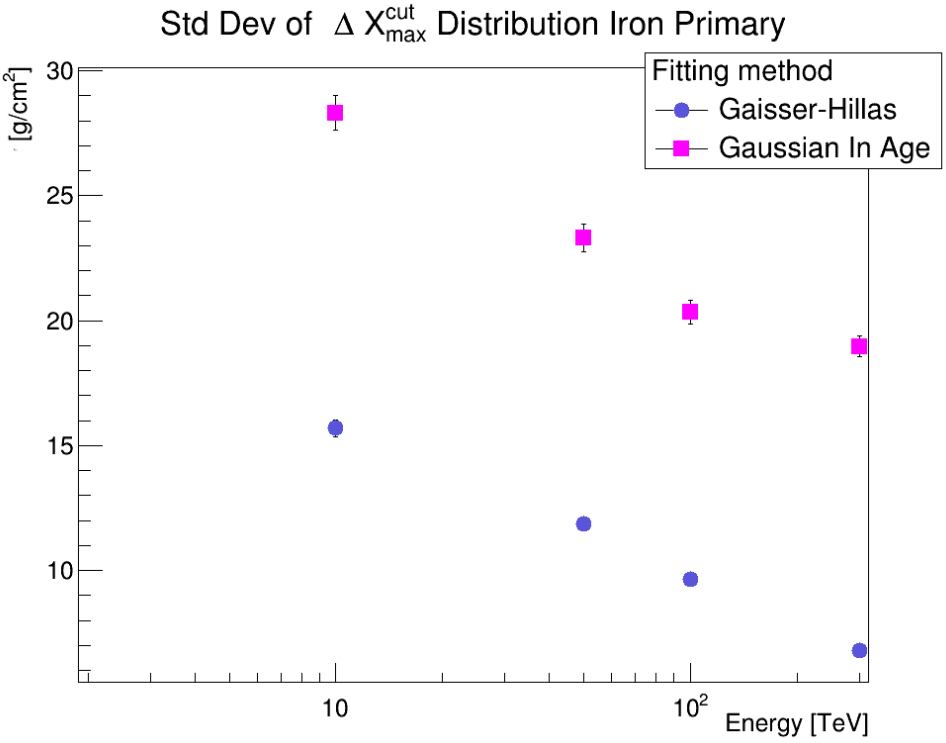

Figure 19: The standard deviation of the difference between the full profile, X_{max}, and the cut profile, X^*_{max}, for both the Gaisser-Hillas and Gaussian in Age function when fitted on the iron primary particle

It do has to be said that due to how the restricted range is determined to be different for each event there will be slight variations in the exact values of both the Mean and Standard deviation shown in Figure 20 and Figure 21. These variations however are not substantial enough to warrant any invalidation of the conclusions gotten through these methods.

5 Results: Discussion

In this segment of the results there will be a more detailed and in depth discussion on what has been shown previously.

5.1 X_{max} distributions

Table 2 contains the more precise values of the Mean from the difference between GH and GIA functions for each primary particle at different energies. As mentioned earlier, the two different fitting methods will agree more about the position of the maximum longitudinal depth, X_{max}, the closer the Mean value is to zero. Looking at Figure 14 and the values in Table 2 one can observe that for both the Iron and Proton primary particle, when fitted on the Full Shower Profile, there is little disagreement between the two fitting methods with both staying within a value of approximately 1 g/cm^2 from each other. Looking at the values of X_{max} in table 1, and in particular the error of those values. One sees that these are close to, if not larger, than the difference of the two Functions. Therefore it seems that when a Full Shower Profile is available it is inconsequential which of the two fitting methods is applied. It is still of interest to note that solely for the Iron primary particle the Gaussian In Age function estimates X_{max} to be at a higher depth than the Gaisser-Hillas function, hence the reason for negative values in Table 1.

Mean Value $X_{max}^{GH} - X_{max}^{GIA}$ distribution in g/cm^2			
Energy	Iron	γ	Proton
10 TeV	-0.7417 $\pm$ 0.07852	2.8792 $\pm$ 0.15287	0.7323 $\pm$ 0.20793
50 TeV	-0.1379 $\pm$ 0.07646	3.1549 $\pm$ 0.13198	0.9344 $\pm$ 0.19530
100 TeV	-0.0806 $\pm$ 0.08615	3.2302 $\pm$ 0.12534	0.8345 $\pm$ 0.12534
300 TeV	-0.0522 $\pm$ 0.08095	3.2043 $\pm$ 0.12437	0.7795 $\pm$ 0.16851

Table 2: The Mean values for the difference of maximum position X_{max} between the Gaisser-Hillas fitting method and the Gaussian In Age fitting method when applied on the Full Shower Profile

5.2 ΔX_{max}^{cut} distributions

For the Full Shower Profile it did not matter which of the two models was used to determine the maximum longitudinal depth. The same can not be said however for when one is considering a restricted or cut profile. A low value for the mean of that distribution would thus imply a lower dependence on choice of fit range and thus would prove to be more reliable to deliver accurate results when only part of the Shower Profile is detected, as tends to happen when working with non-simulated Air Showers. In figure 18 it is apparent that the Iron primary particle favours one of the two fitting methods, in this case the Gaisser-Hillas function. Similarly for the Photon as primary particle, Figure

49, the GH function is shown to deliver more reliable and robust results. The only exception for this would be the Proton primary, Figure 50, at 100 TeV and 300 TeV where the GIA function seems to be slightly more accurate. On top of accuracy the GH function tends to deliver more precise results for in comparison to its Gaussian counterpart when being applied to the Iron primary. Figure 19 shows the standard deviation for both fitting methods. A lower value for the standard deviation implies a more stable belief in the results which shows there is an higher stability in the Gaisser-Hillas function than the Gaussian in Age function when under the effect of cut profiles. Additionally the same is true for the Photon and Proton when being used as primary particle.
Thus it seems that in the scenario of restricted shower profiles the Gaisser-Hillas function describes the different longitudinal profiles in a more accurate and precise way, regardless of fit range, particle type, and energy.

6 Conclusion

The longitudinal development of air showers in the atmosphere is used as a means to infer the properties of cosmic rays of the highest energies, where space-based detection is not possible due to the extremely low fluxes. In particular the shower maximum, X_{max} is connected to the energy and mass composition of the cosmic rays' primary particle. In this work, characterisation of the shower profile in the TeV range has been performed, adding a tiny but relevant piece of information towards the understanding of the cosmic ray mass composition with ground-based observatories.
The ROOT framework was used to analyse simulated showers generated with the `CONEX` simulation package. Two trial functions, the Gaisser-Hillas function and the Gaussian in Age function, have been used to characterise the longitudinal development of the shower profile and to obtain the shower maximum X_{max}. The goal was to investigate which function better describes the shower profiles of the different particles (γ rays, protons and iron nuclei) and at different energies (10 TeV, 50 TeV, 100 TeV, 300 TeV). Moreover, testing of the stability of the results against different fit ranges to test the effect of the tails of the profiles at both very low and very high atmospheric depths.
When fitting over the whole range of atmospheric depth, both functions are equally good at describing the shower maximum for gamma rays, protons and iron nuclei over all the energies investigated. In particular, the showers initiated by cosmic-ray iron primaries are practically insensitive to the parametrization, with no sizeable difference found in the shower axis value. Showers initiated by gamma rays and cosmic ray protons do show some between the two parametrizations, but this difference is small compared to the sensitivity of the method.
The second part of the study consists in introducing a range in the fit and comparing the results of the fit with the previous result obtained from the fit to the full range. The results of this second step indicate that when looking at showers generated by a cosmic-ray iron, the Gaisser-Hillas function is less sensitive to the tails, and thus it is more suitable to further studies of cosmic-ray composition over all the considered energies. This can be seen by both the mean and the standard deviation distributions. For primary photons, the situation is distinctly different since the Gaussian in age is the parametrisation which shows the smaller difference and thus is less sensitive to the tails. For primary protons, the situation is even different, with the two parametrisations giving essentially the same result, both at the level of the mean and the standard deviation. A thorough investigation of the causes of these different results is beyond the scope of this work, but it should be looked for in the fluctuations of the shower shape that is profoundly different for the three primary species that we considered.

Bibliography

[1] Thoudam, S., Rachen, J. P., van Vliet, A., Achterberg, A., Buitink, S., Falcke, H., and Hörandel, J. R., "Cosmic-ray energy spectrum and composition up to the ankle: the case for a second galactic component," *A&A*, vol. 595, p. A33, 2016.

[2] L. Baldini, "Space-based cosmic-ray and gamma-ray detectors: a review," 2014.

[3] M. Rao and B. Sreekantan, *Extensive Air Showers*. World Scientific, 1998.

[4] W. Heitler, *24. Cascade Showers*, p. 232–239. Oxfort University Press, ed. 2 ed., 1944.

[5] J. A. Aguilar, "Particle astrophysics lecture 3."

[6] A. Berg and M. Vecchi, "Particle detection in astroparticle physics," Jan 2021.

[7] A. Haungs, H. Rebel, and M. Roth, "Energy spectrum and mass composition of high-energy cosmic rays," *Reports on Progress in Physics*, vol. 66, pp. 1145–1206, jun 2003.

[8] R. Ulrich, R. Engel, and M. Unger, "Hadronic multiparticle production at ultrahigh energies and extensive air showers," *Phys. Rev. D*, vol. 83, p. 054026, Mar 2011.

[9] J. Albrecht, L. Cazon, H. Dembinski, A. Fedynitch, K.-H. Kampert, T. Pierog, W. Rhode, D. Soldin, B. Spaan, R. Ulrich, and M. Unger, "The muon puzzle in cosmic-ray induced air showers and its connection to the large hadron collider," *Astrophysics and Space Science*, vol. 367, 03 2022.

[10] R. Brun and F. Rademakers, *ROOT - An object Orientated Data Analysis Framework*. Proceedings AIHENP '96 Workshop, Laussane, Sep. 1996, Nucl. Inst. Meth. in Phys. Res. A 389 (1997) 81-86., v.6.26.02 13/04/2022.

[11] C. Lattner and V. Adve, "LLVM: A compilation framework for lifelong program analysis and transformation," (San Jose, CA, USA), pp. 75–88, Mar 2004.

[12] "Clang: A c language family frontend for llvm."

[13] T. Bergmann *et al.*, "One-dimensional hybrid approach to extensive air shower simulation," *Astropart. Phys.*, vol. 26, pp. 420–432, 2007.

[14] T. Pierog *et al.*, "First results of fast one-dimensional hybrid simulation of eas using conex," *Nucl. Phys. Proc. Suppl.*, vol. 151, pp. 159–162, 2006.

[15] S. Ostapchenko, "QGSJET-II: Towards reliable description of very high energy hadronic interactions," *Nucl. Phys. B Proc. Suppl.*, vol. 151, pp. 143–146, 2006.

[16] M. Bleicher, E. Zabrodin, C. Spieles, S. A. Bass, C. Ernst, S. Soff, L. Bravina, M. Belkacem, H. Weber, H. Stöcker, and W. Greiner, "Relativistic hadron-hadron collisions in the ultra-relativistic quantum molecular dynamics model," *Journal of Physics G: Nuclear and Particle Physics*, vol. 25, pp. 1859–1896, sep 1999.

[17] A. M. Hillas, *Cosmic Rays*. Selected Readings in Physics S., London, England: Pergamon Press, Aug. 1972.

[18] T. K. Gaisser and A. M. Hillas, "Reliability of the Method of Constant Intensity Cuts for Reconstructing the Average Development of Vertical Showers," in *International Cosmic Ray Conference*, vol. 8 of *International Cosmic Ray Conference*, p. 353, Jan. 1977.

[19] T. Abu-Zayyad, K. Belov, D. Bird, J. Boyer, Z. Cao, M. Catanese, G. Chen, R. Clay, C. Covault, H. Dai, B. Dawson, J. Elbert, B. Fick, L. Fortson, J. Fowler, K. Gibbs, M. Glasmacher, K. Green, Y. Ho, and X. Zhang, "A measurement of the average longitudinal development profile of cosmic ray air showers between 1017 and 1018 ev," *Astroparticle Physics*, vol. 16, p. 1–11, 10 2001.

[20] A. Rotenberg, "A new pseudo-random number generator," *J. ACM*, vol. 7, p. 75–77, jan 1960.

Appendices

A Plots

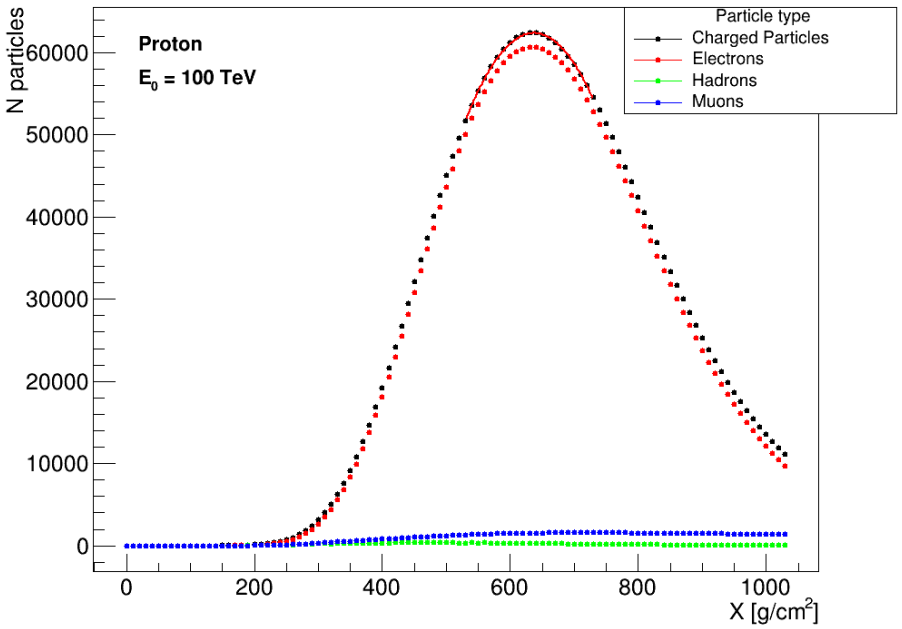

Figure 20: Shower development of a single event with Proton primary at 100 TeV

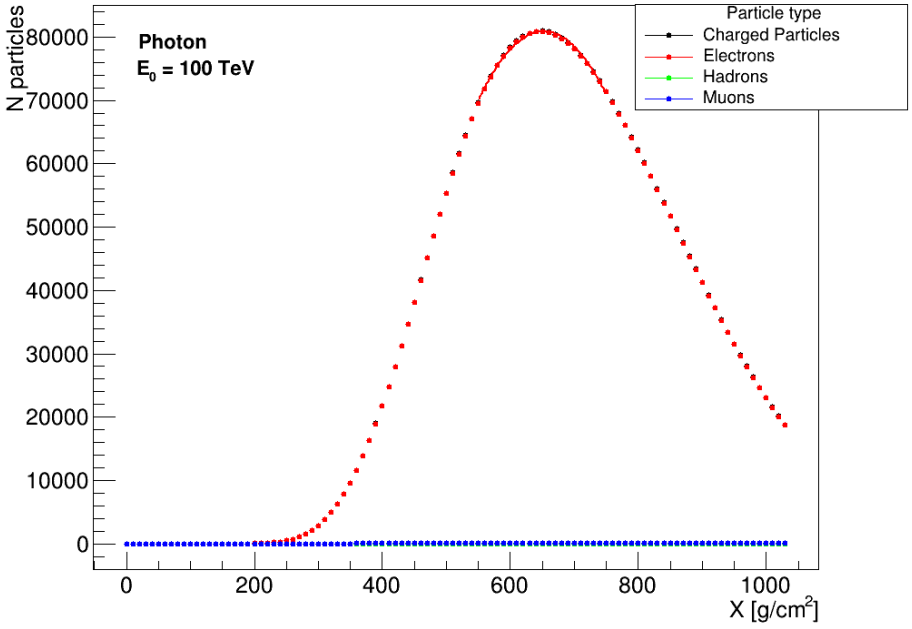

Figure 21: Shower development of a single event with γ primary at 100 TeV

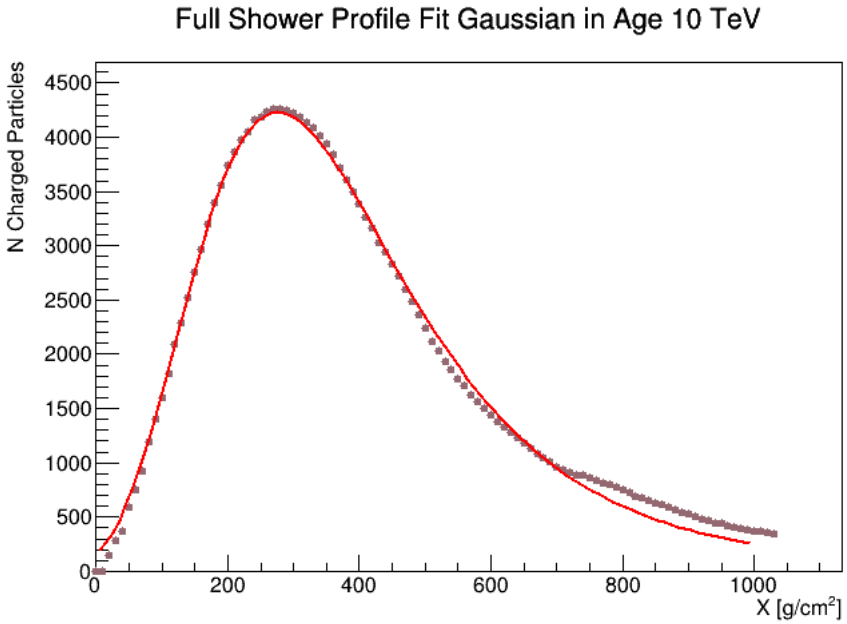

Figure 22: Gaussian in Age function fitted over the full profile of an Iron primary particle

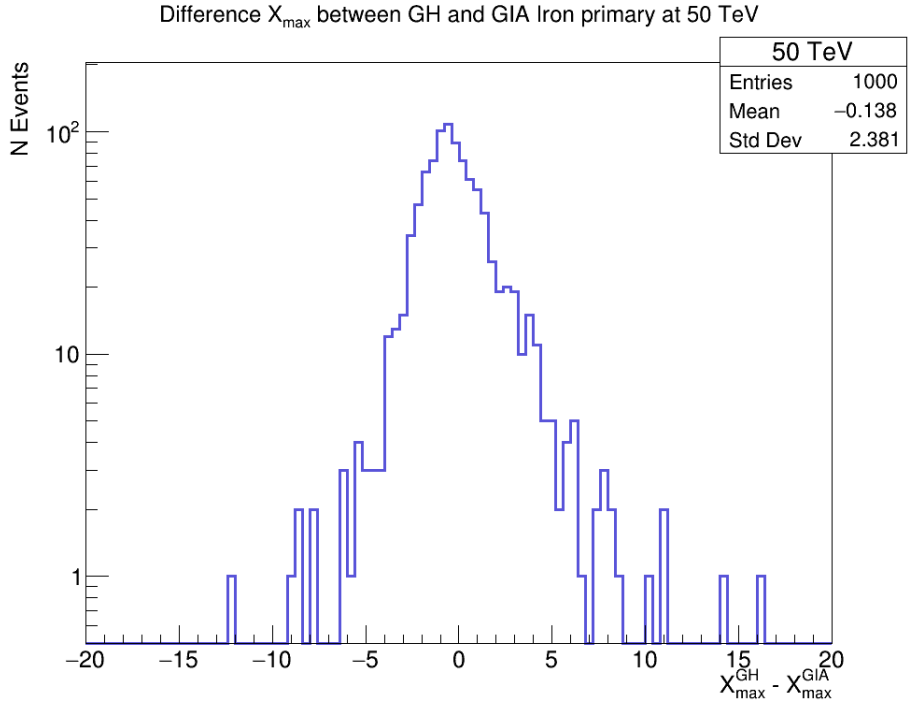

Figure 23: 1-D distribution of the difference for the position of Xmax between the Gaisser-Hillas function and the Gaussian in Age function when fitted over the full shower profile of a iron primary particle at 50 TeV

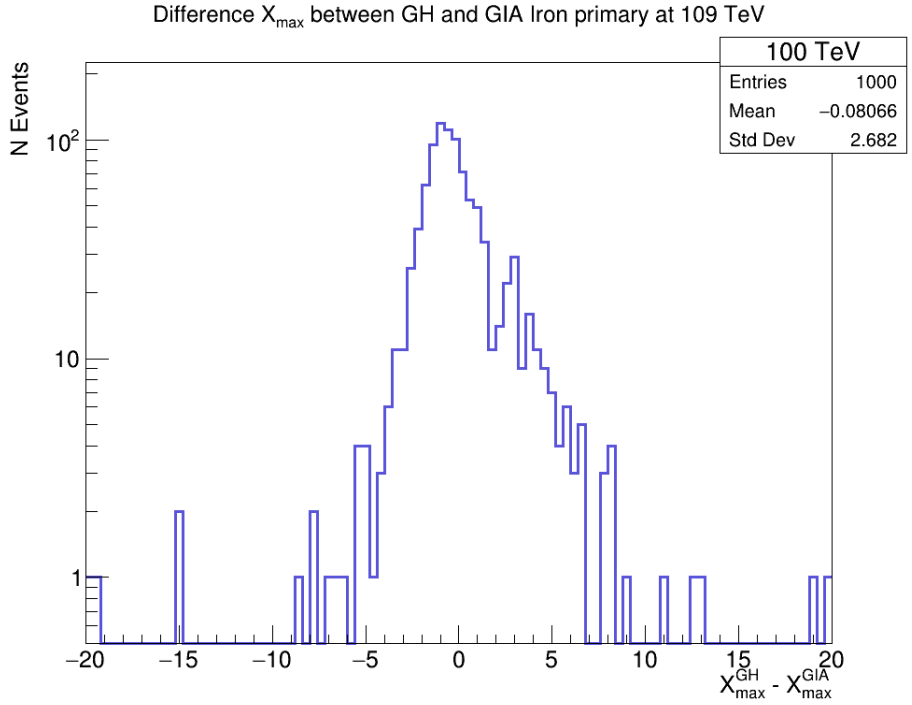

Figure 24: 1-D distribution of the difference for the position of Xmax between the Gaisser-Hillas function and the Gaussian in Age function when fitted over the full shower profile of a iron primary particle at 100 TeV

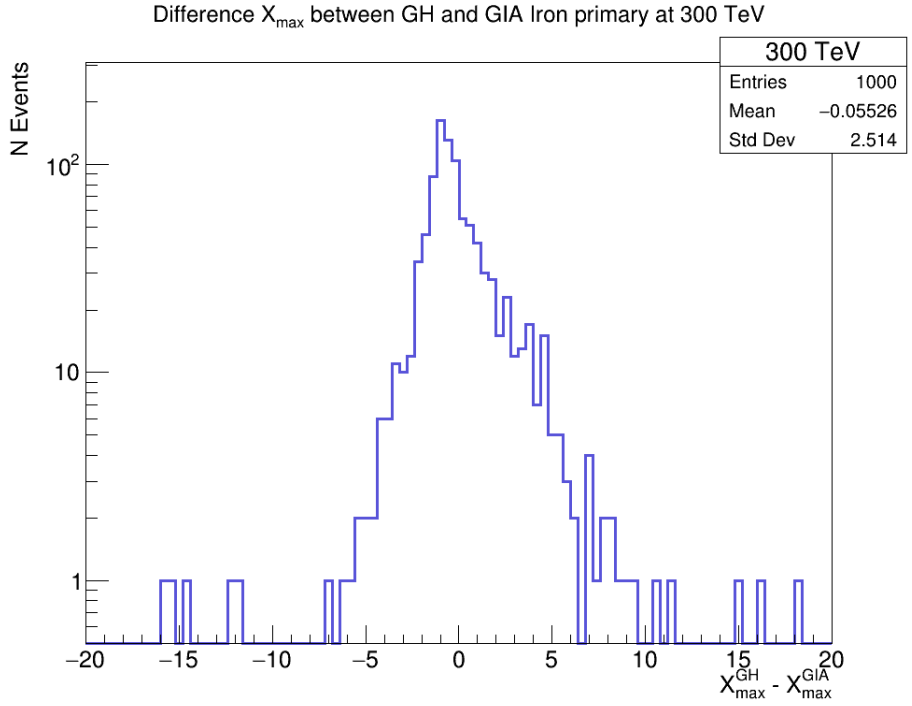

Figure 25: 1-D distribution of the difference for the position of Xmax between the Gaisser-Hillas function and the Gaussian in Age function when fitted over the full shower profile of a iron primary particle at 300 TeV

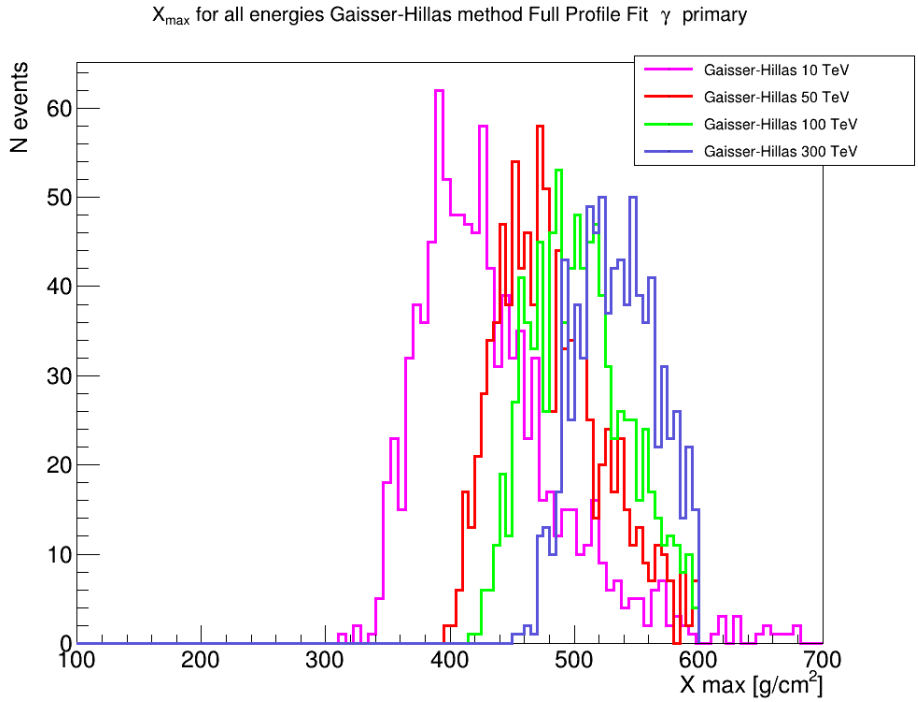

Figure 26: Histograms of the 1-D distribution of maximum longitudinal depth, X_{max}, for the γ Primary particle using multiple energies fitted using the Gaisser-Hillas function on the entire shower profile.

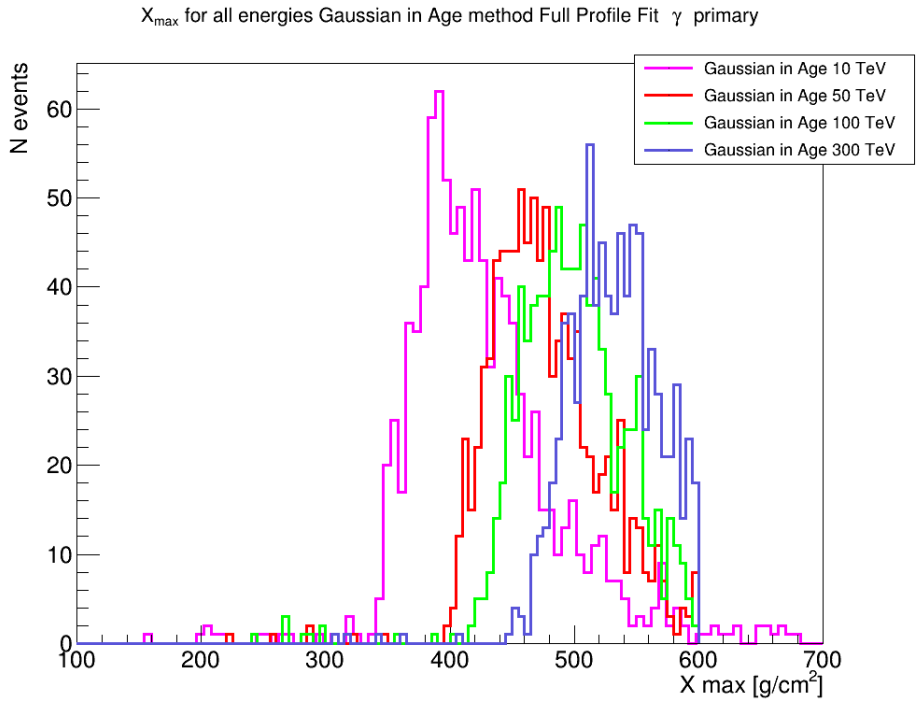

Figure 27: Histogram of the 1-D distribution of maximum longitudinal depth, Xmax, for the γ Primary particle using multiple energies fitted using the Gaussian In Age function on the entire shower profile.

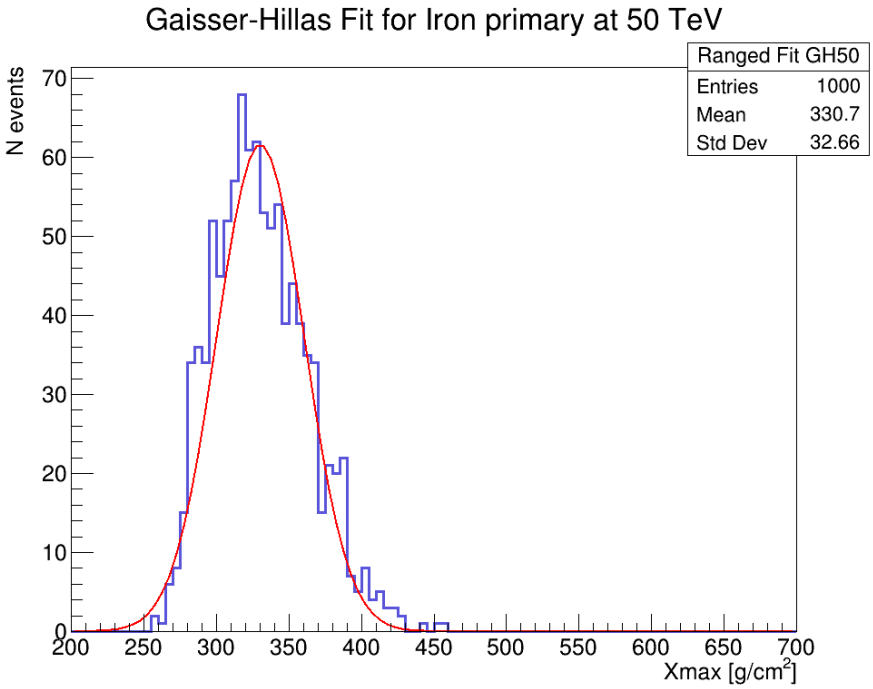

Figure 28: Histogram of the 1-D distribution of maximum longitudinal depth determined, X^*_{max} by the Gaisser-Hillas function for the Iron Primary Particle at 50 TeV when fitted to a restricted range of the shower profile.

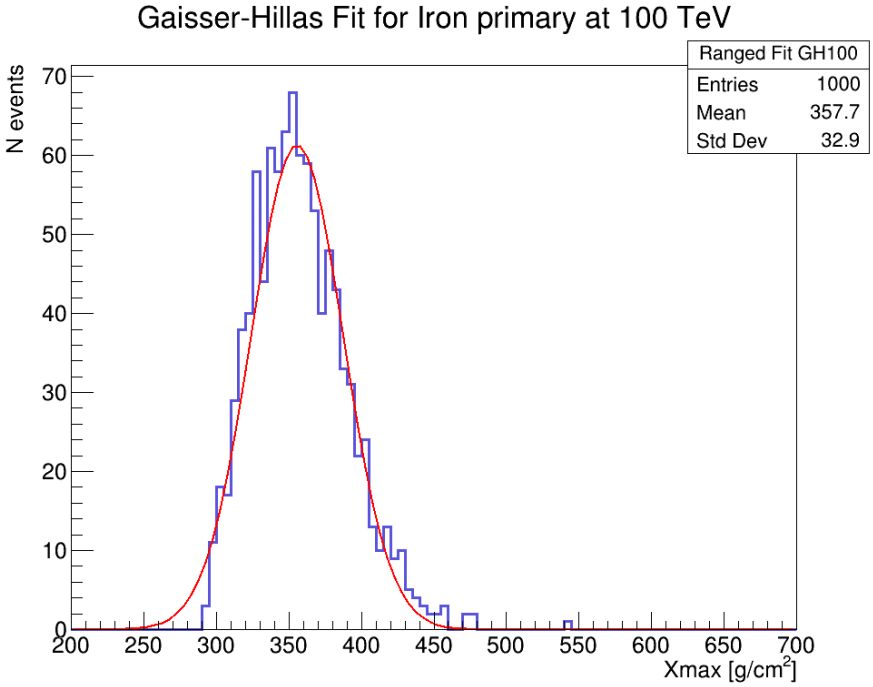

Figure 29: Histogram of the 1-D distribution of maximum longitudinal depth determined, X^*_{max} by the Gaisser-Hillas function for the Iron Primary Particle at 100 TeV when fitted to a restricted range of the shower profile

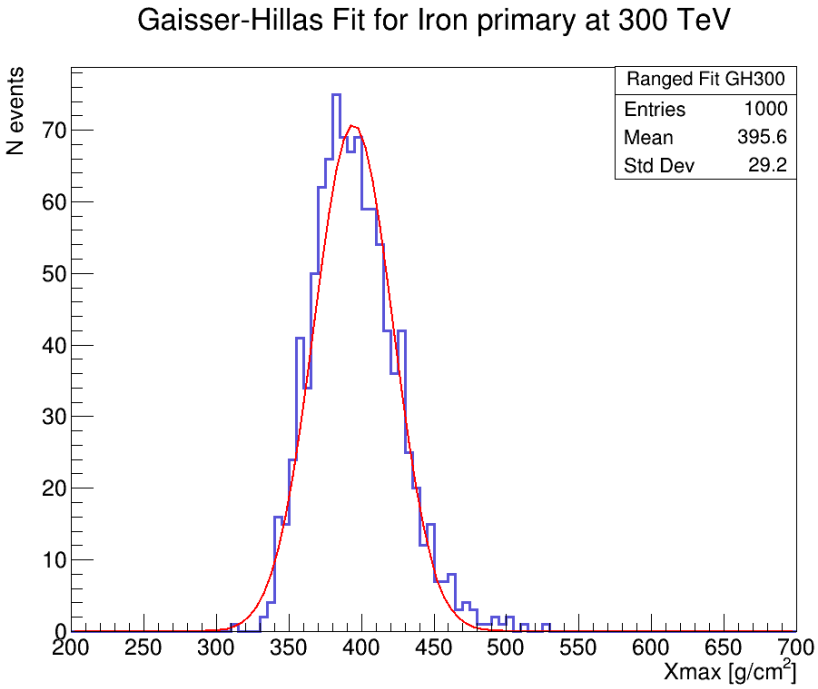

Figure 30: Histogram of the 1-D distribution of maximum longitudinal depth determined, X^*_{max} by the Gaisser-Hillas function for the Iron Primary Particle at 300 TeV when fitted to a restricted range of the shower profile

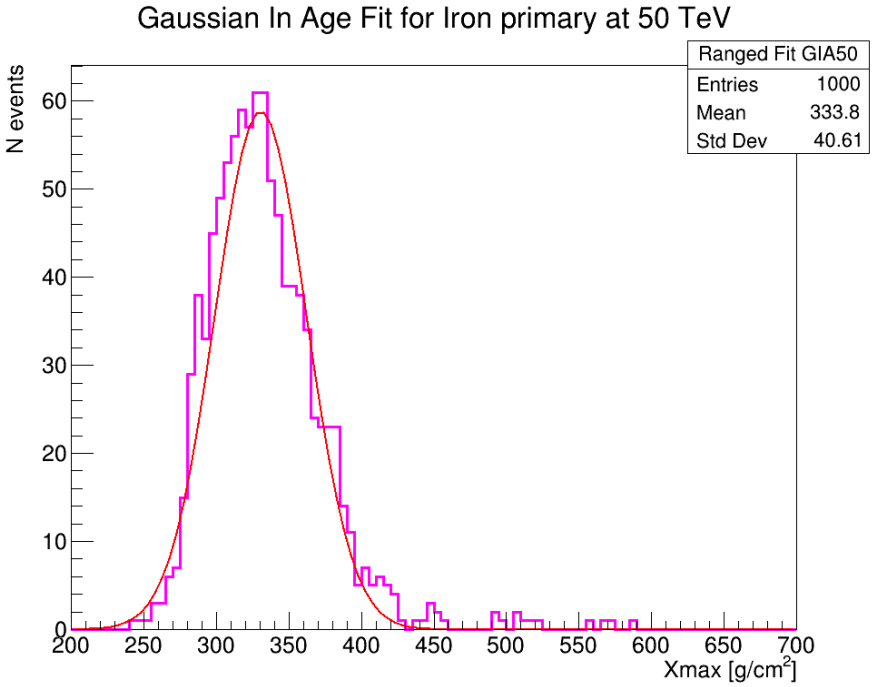

Figure 31: Histogram of the 1-D distribution of maximum longitudinal depth determined, X^*_{max} by the Gaussian in Age function for the Iron Primary Particle at 50 TeV when fitted to a restricted range of the shower profile.

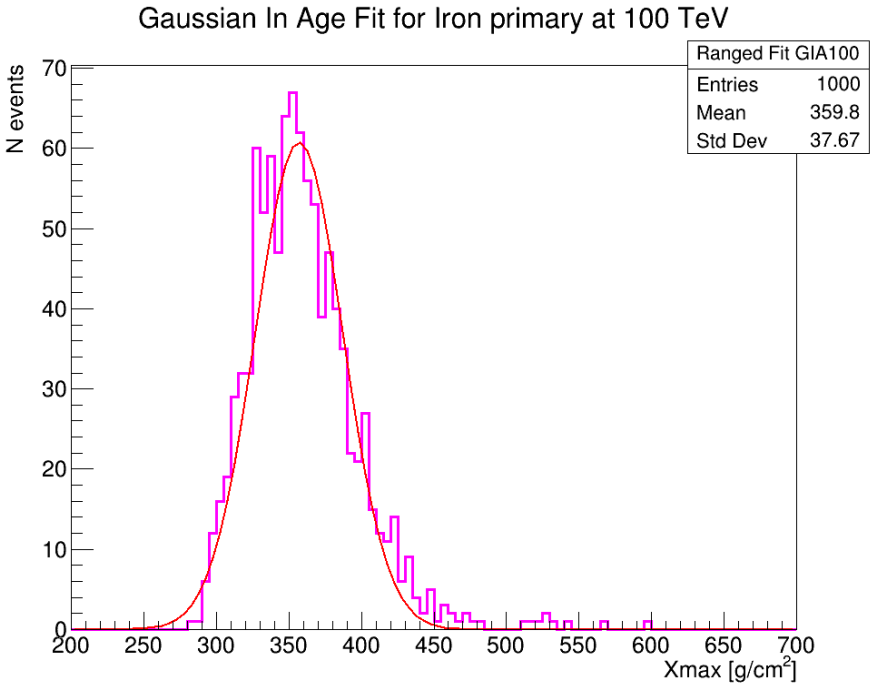

Figure 32: Histogram of the 1-D distribution of maximum longitudinal depth determined, X^*_{max} by the Gaussian in Age function for the Iron Primary Particle at 100 TeV when fitted to a restricted range of the shower profile

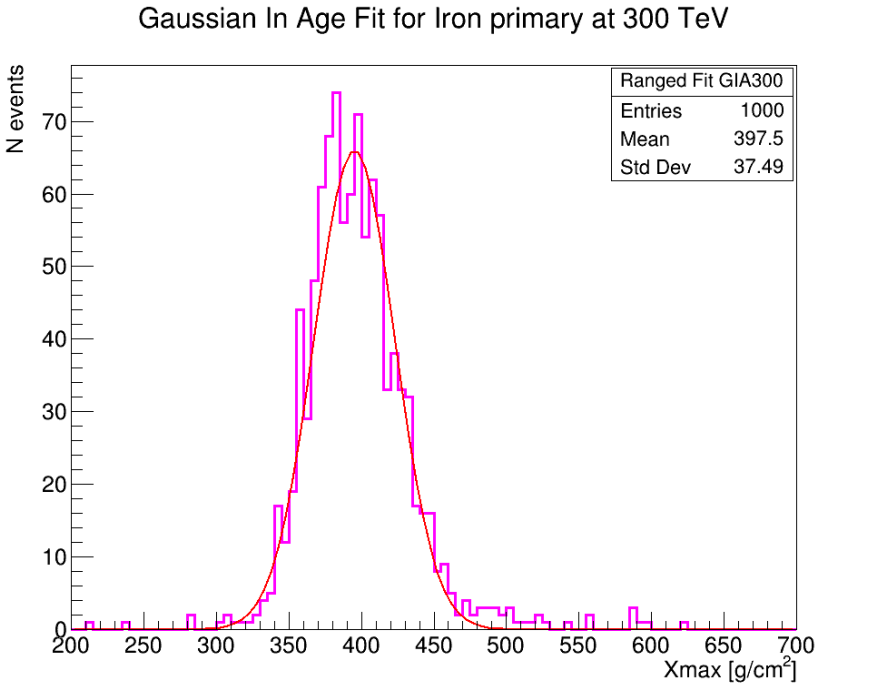

Figure 33: Histogram of the 1-D distribution of maximum longitudinal depth determined, X^*_{max} by the Gaussian in Age function for the Iron Primary Particle at 300 TeV when fitted to a restricted range of the shower profile

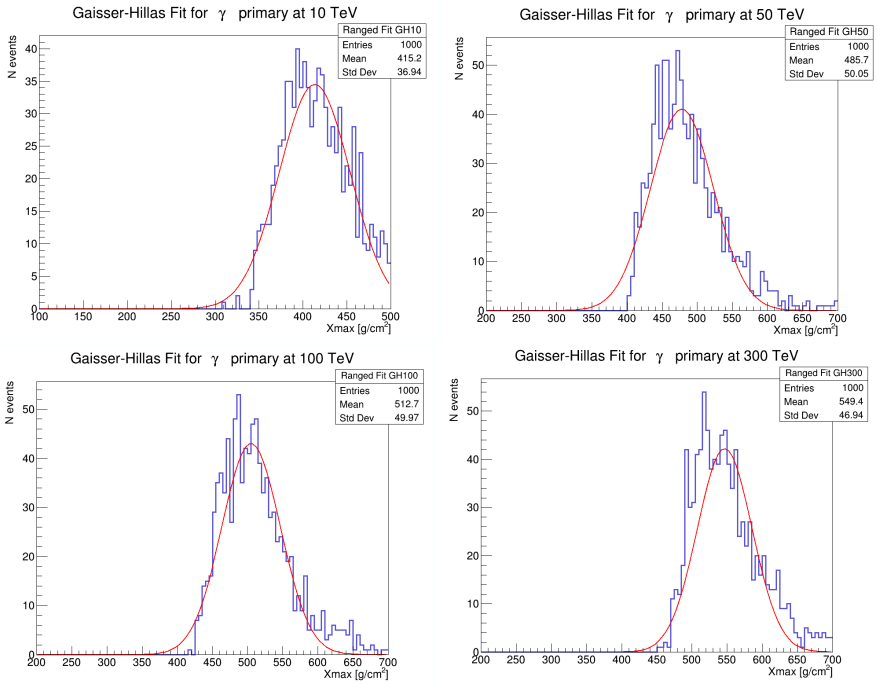

Figure 34: Histograms of the 1-D distribution of maximum longitudinal depth determined, X^*_{max} by the Gaisser-Hillas function for the photon Primary Particle when fitted to a restricted range of the shower profile.
a) Energy of 10 TeV, b) Energy of 50 TeV, c) Energy of 100 TeV, d) Energy of 300 TeV

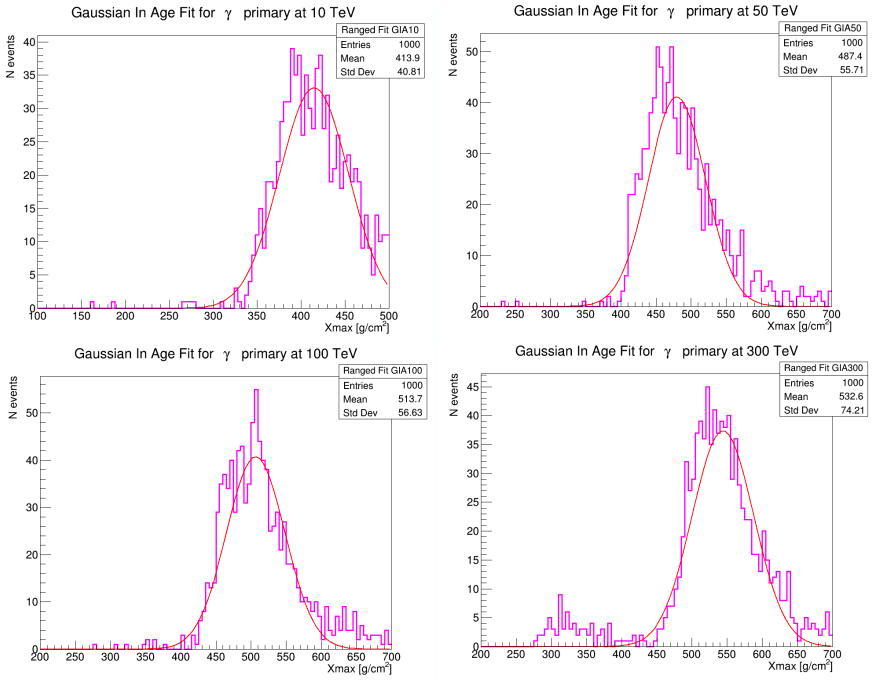

Figure 35: Histograms of the 1-D distribution of maximum longitudinal depth determined, X^*_{max} by the Gaussian in Age function for the photon Primary Particle when fitted to a restricted range of the shower profile.
a) Energy of 10 TeV, b) Energy of 50 TeV, c) Energy of 100 TeV, d) Energy of 300 TeV

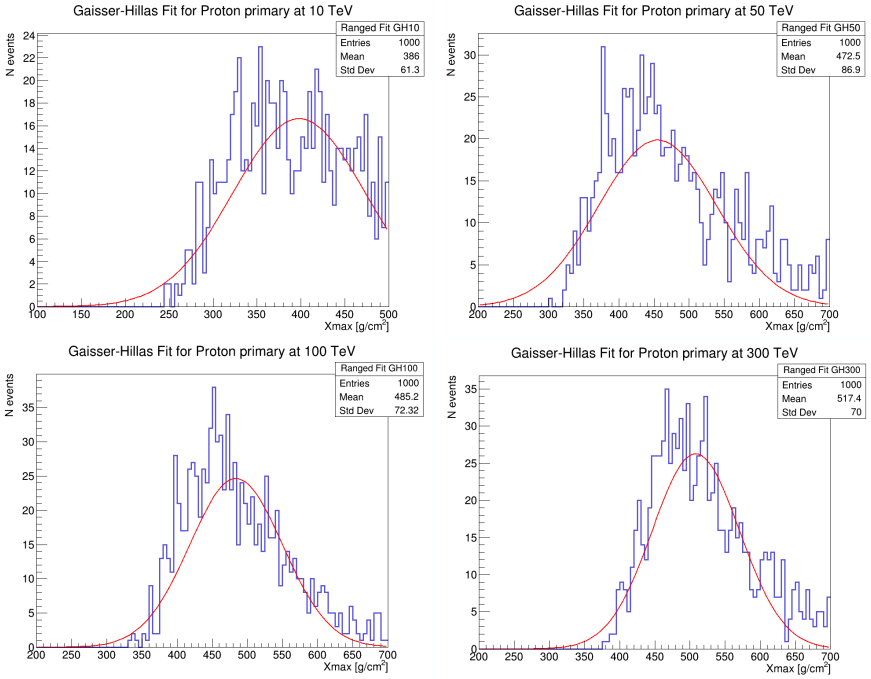

Figure 36: Histograms of the 1-D distribution of maximum longitudinal depth determined, X^*_{max} by the Gaisser-Hillas function for the proton Primary Particle when fitted to a restricted range of the shower profile.
a) Energy of 10 TeV, b) Energy of 50 TeV, c) Energy of 100 TeV, d) Energy of 300 TeV

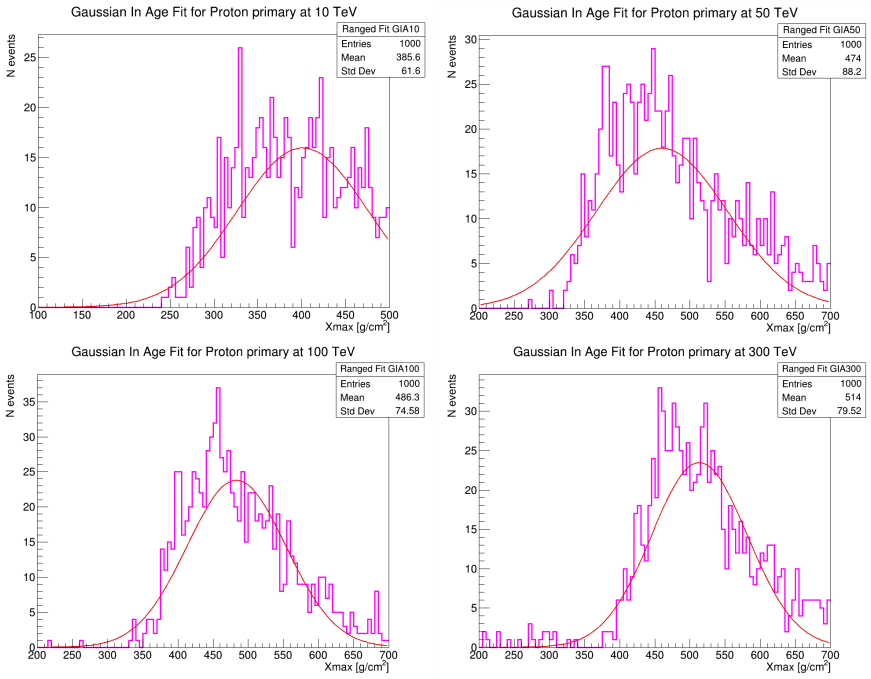

Figure 37: Histograms of the 1-D distribution of maximum longitudinal depth determined, X^*_{max} by the Gaussian in Age function for the proton Primary Particle when fitted to a restricted range of the shower profile.
a) Energy of 10 TeV, b) Energy of 50 TeV, c) Energy of 100 TeV, d) Energy of 300 TeV

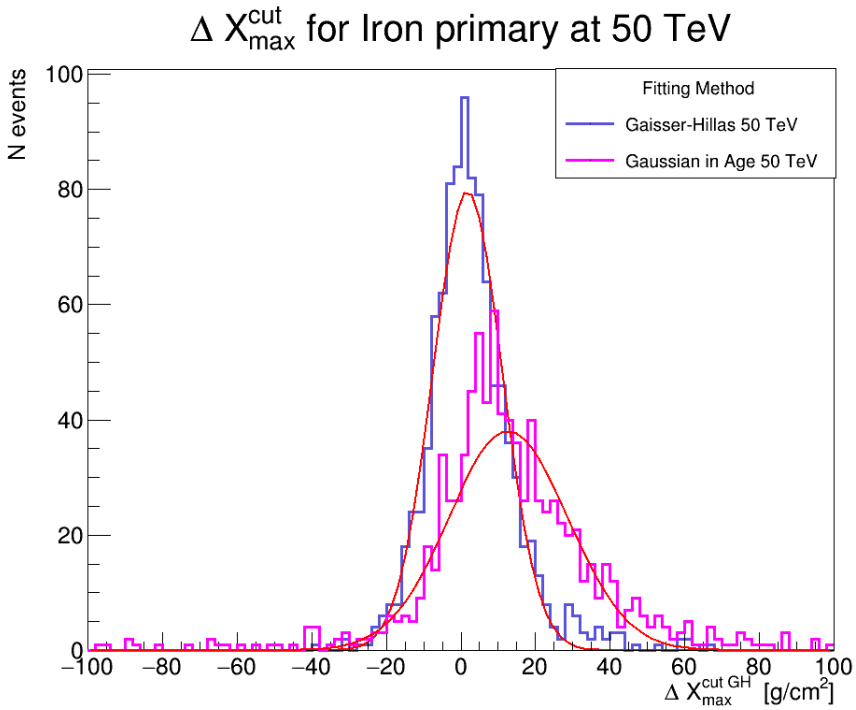

Figure 38: Histogram of the 1-D distribution of ΔX_{max}^{cut} for both the Gaisser-Hillas and Gaussian In Age function for the Iron Primary Particle at 50 TeV.

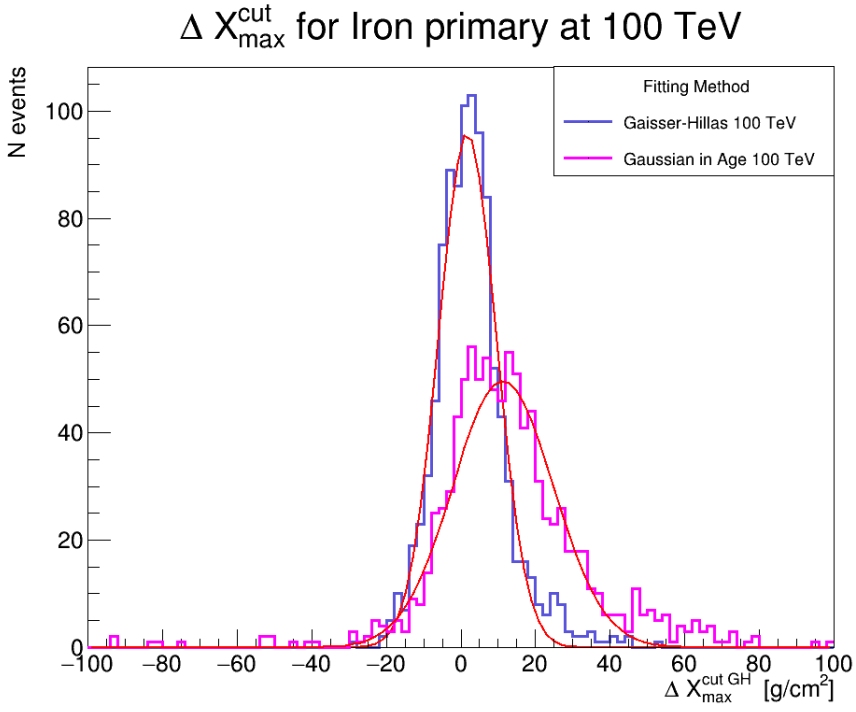

Figure 39: Histogram of the 1-D distribution of ΔX_{max}^{cut} for both the Gaisser-Hillas and Gaussian In Age function for the Iron Primary Particle at 100 TeV.

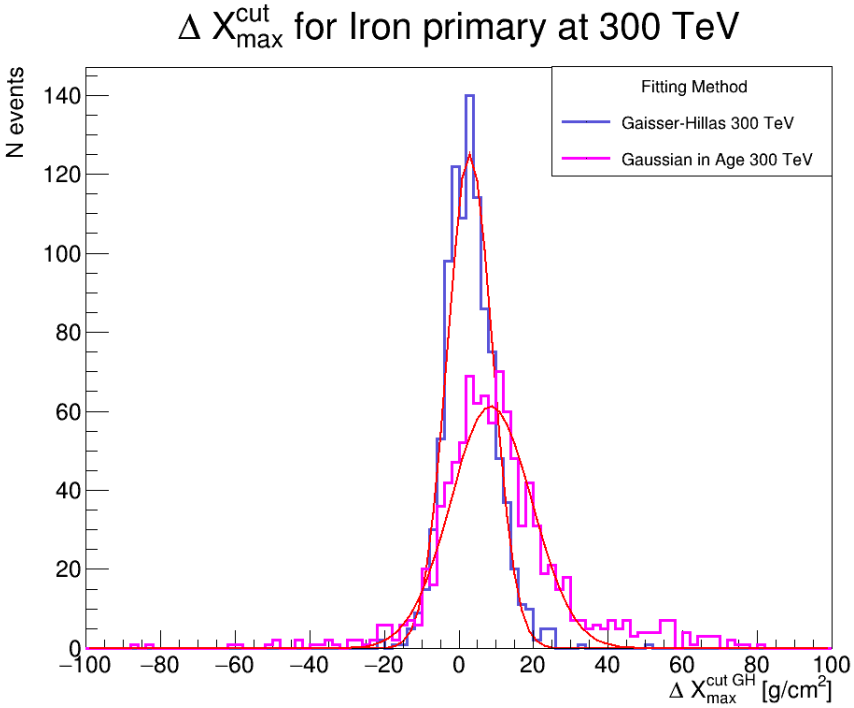

Figure 40: Histogram of the 1-D distribution of ΔX_{max}^{cut} for both the Gaisser-Hillas and Gaussian In Age function for the Iron Primary Particle at 300 TeV.

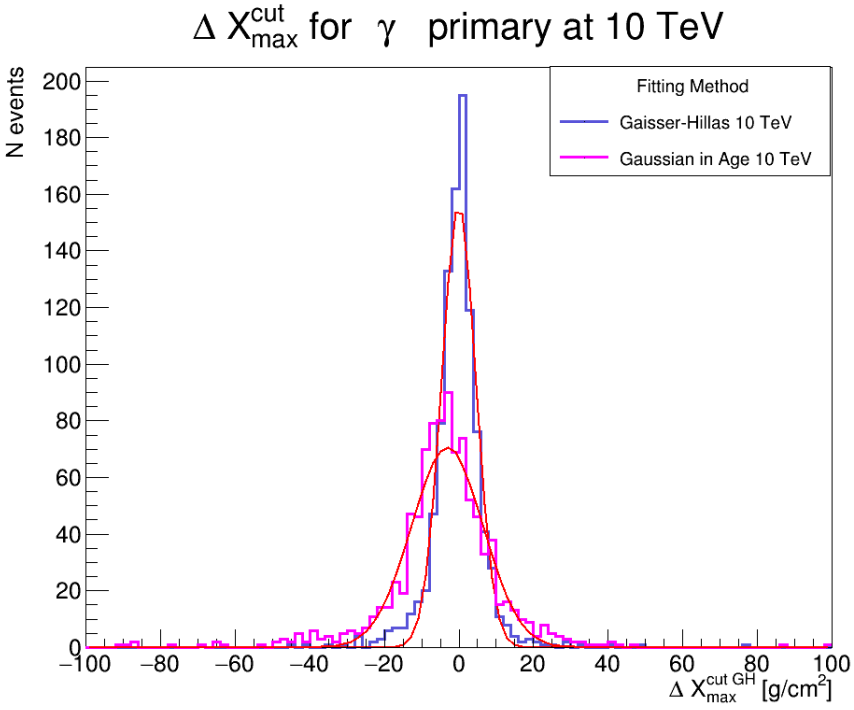

Figure 41: Histogram of the 1-D distribution of ΔX_{max}^{cut} for both the Gaisser-Hillas and Gaussian In Age function for the photon gamma Particle at 10 TeV.

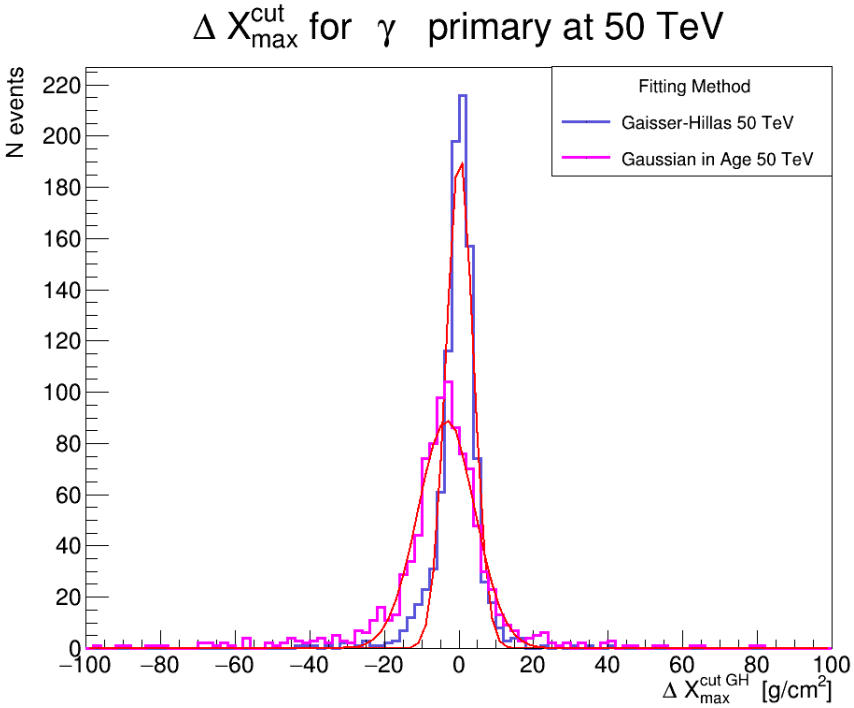

Figure 42: Histogram of the 1-D distribution of ΔX_{max}^{cut} for both the Gaisser-Hillas and Gaussian In Age function for the photon gamma Particle at 50 TeV.

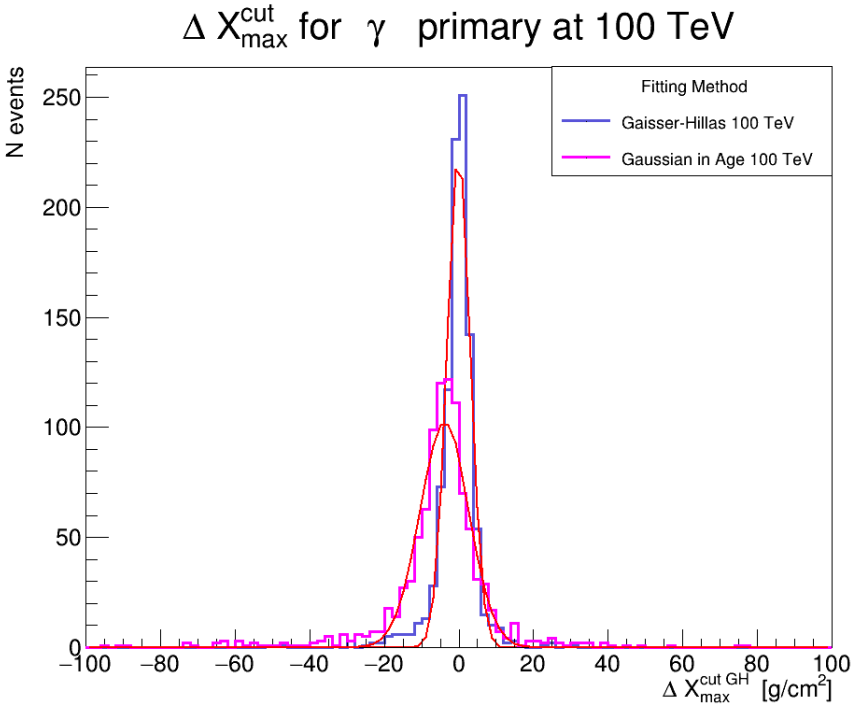

Figure 43: Histogram of the 1-D distribution of ΔX_{max}^{cut} for both the Gaisser-Hillas and Gaussian In Age function for the photon gamma Particle at 100 TeV.

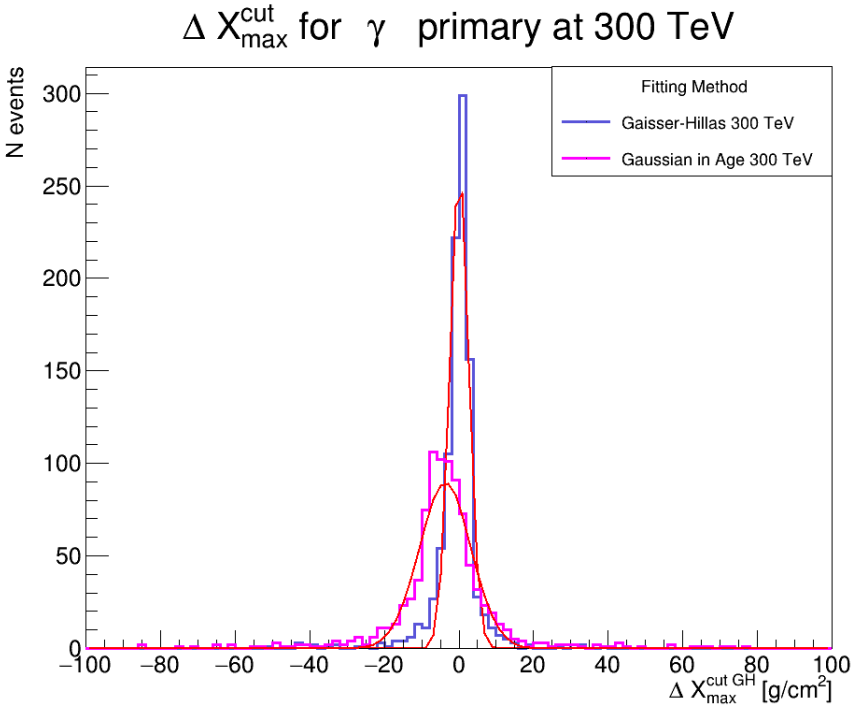

Figure 44: Histogram of the 1-D distribution of ΔX_{max}^{cut} for both the Gaisser-Hillas and Gaussian In Age function for the photon gamma Particle at 300 TeV.

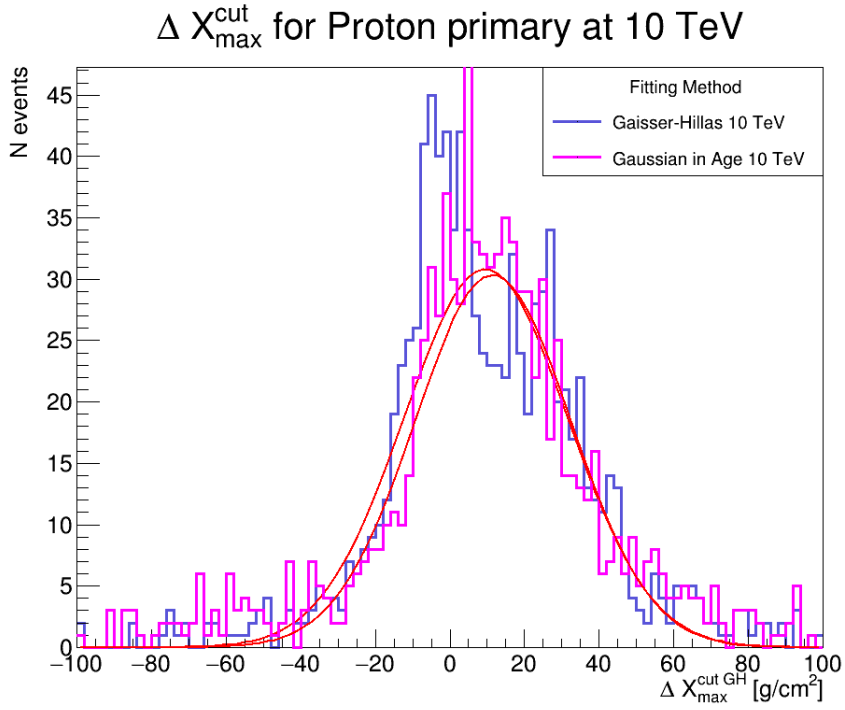

Figure 45: Histogram of the 1-D distribution of ΔX_{max}^{cut} for both the Gaisser-Hillas and Gaussian In Age function for the proton gamma Particle at 10 TeV.

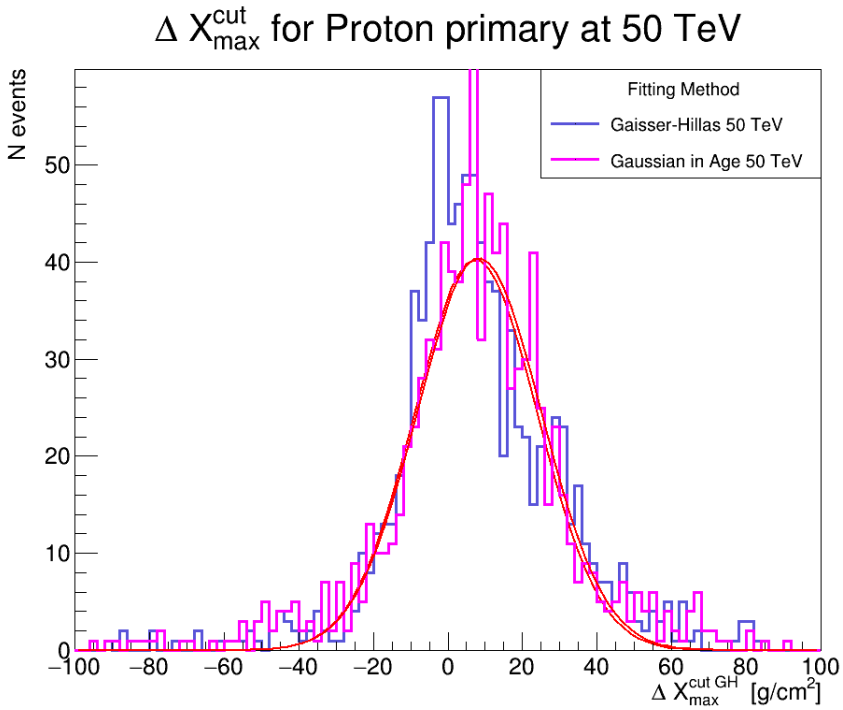

Figure 46: Histogram of the 1-D distribution of ΔX_{max}^{cut} for both the Gaisser-Hillas and Gaussian In Age function for the proton gamma Particle at 50 TeV.

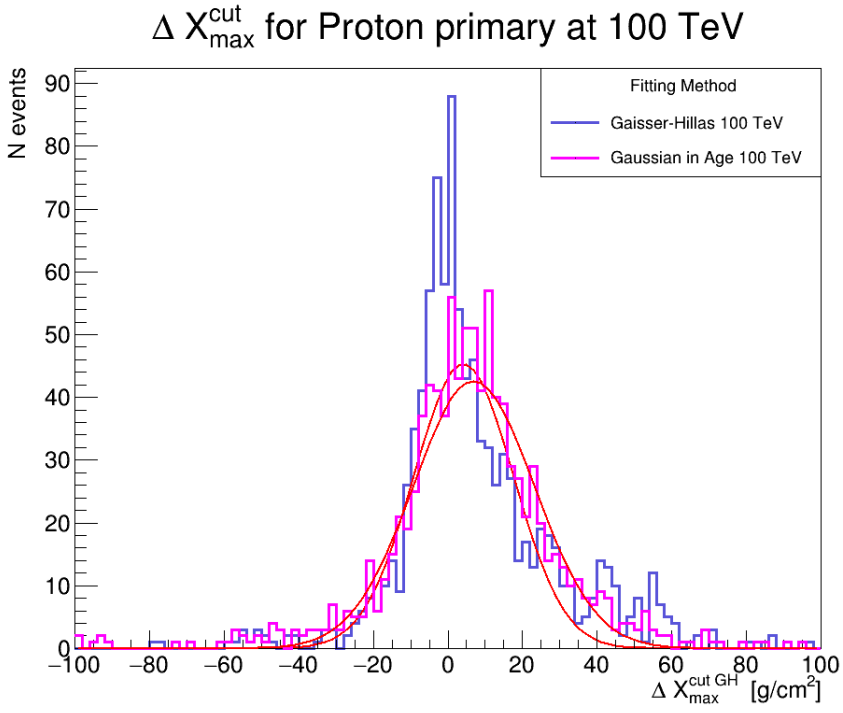

Figure 47: Histogram of the 1-D distribution of ΔX_{max}^{cut} for both the Gaisser-Hillas and Gaussian In Age function for the proton gamma Particle at 100 TeV.

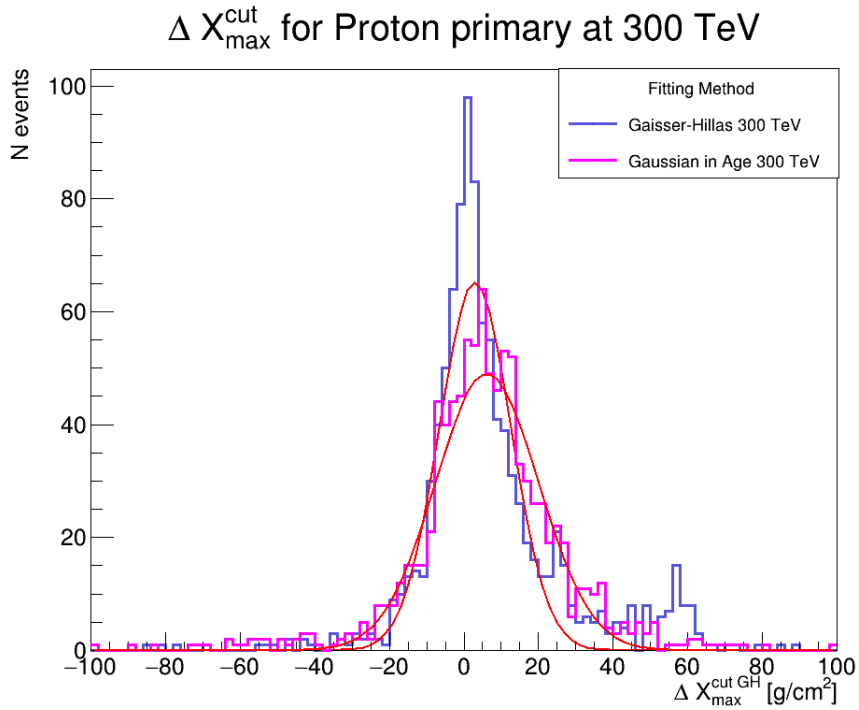

Figure 48: Histogram of the 1-D distribution of ΔX_{max}^{cut} for both the Gaisser-Hillas and Gaussian In Age function for the proton gamma Particle at 300 TeV.

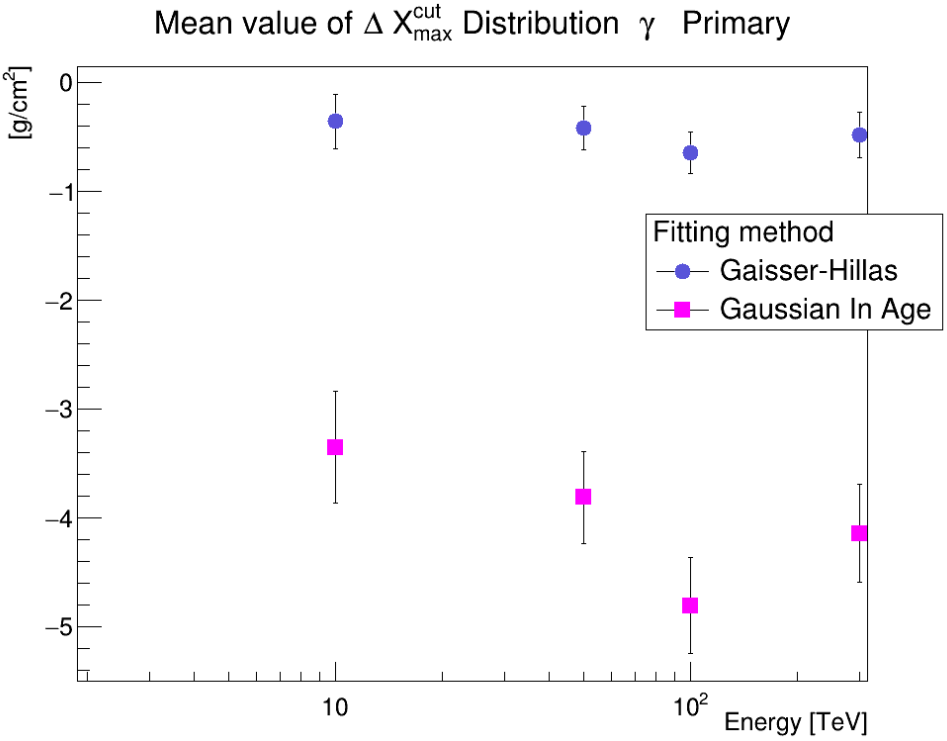

Figure 49: The mean value of the difference between the full profile, X_{max}, and the cut profile, X_{max}^{*}, for both the Gaisser-Hillas and Gaussian in Age function when fitted on a photon primary particle

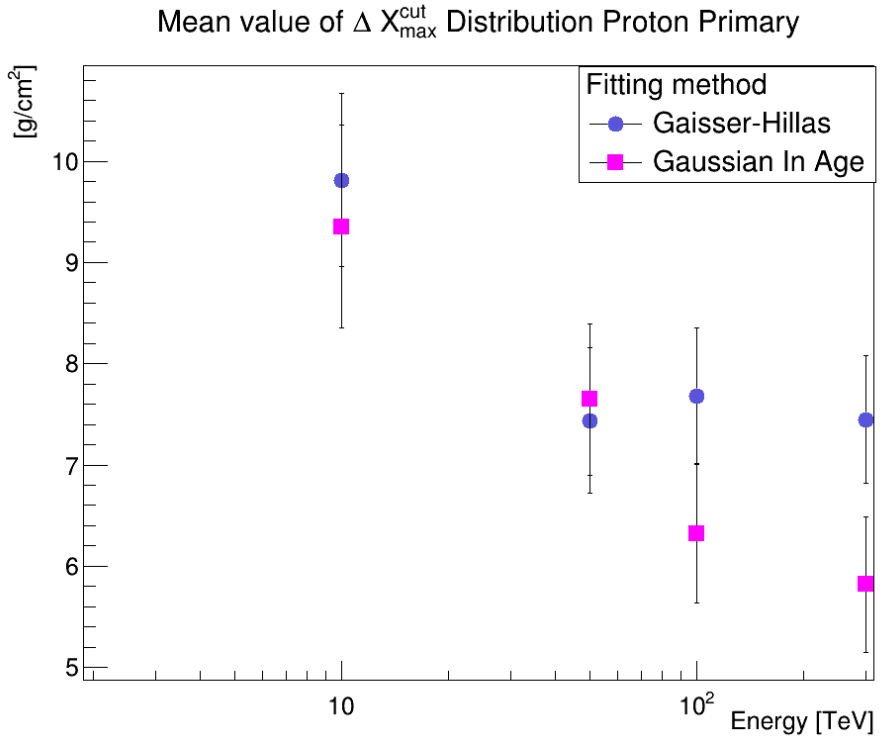

Figure 50: The mean value of the difference between the full profile, X_{max}, and the cut profile, X^*_{max}, for both the Gaisser-Hillas and Gaussian in Age function when fitted on a proton primary particle

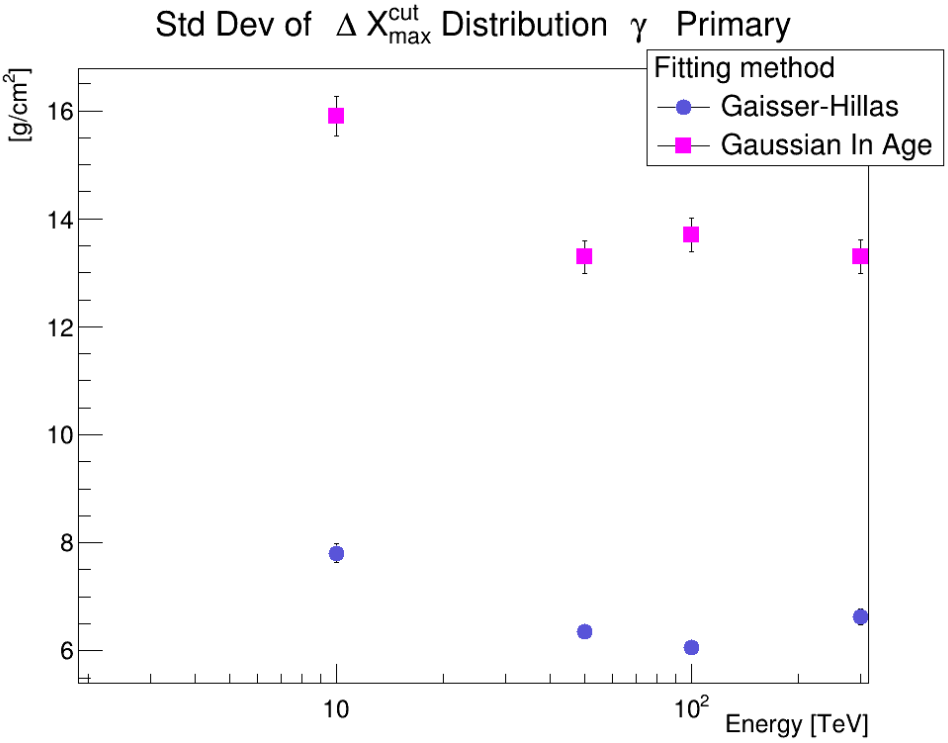

Figure 51: The standard deviation of the difference between the full profile, X_{max}, and the cut profile, X^*_{max}, for both the Gaisser-Hillas and Gaussian in Age function when fitted on a photon primary particle

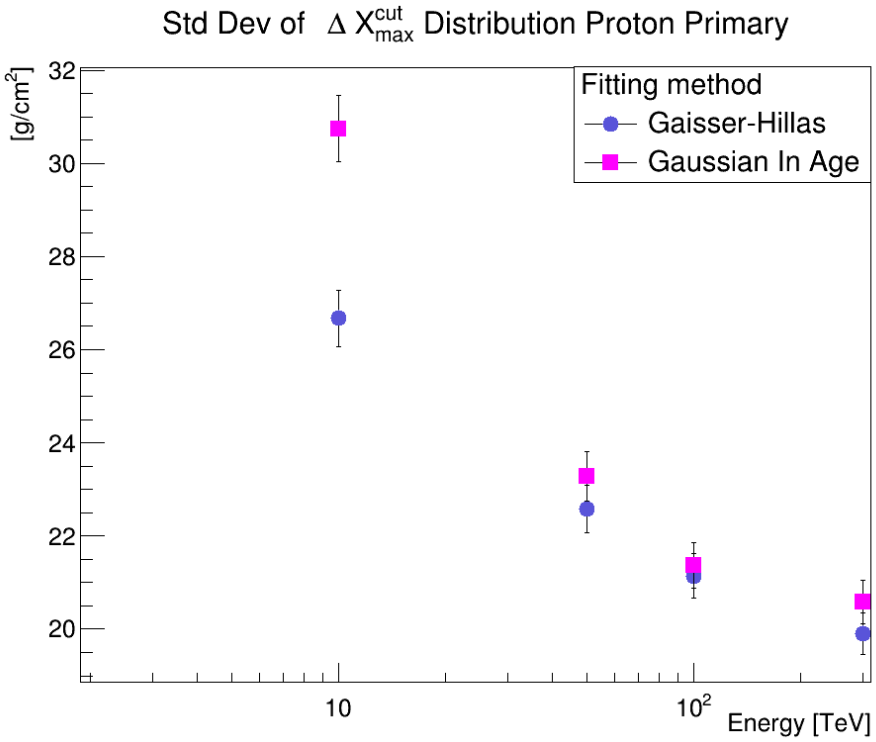

Figure 52: The standard deviation of the difference between the full profile, X_{max}, and the cut profile, X^*_{max}, for both the Gaisser-Hillas and Gaussian in Age function when fitted on a proton primary particle

B Tables

X_{max} Values Photon Primary Particle Full Shower Profile		
Energy	Gaisser-Hillas	Gaussian In Age
10 TeV	431.514 ± 1.81162	426.625 ± 1.94537
50 TeV	481.339 ± 1.35651	475.835 ± 1.49247
100 TeV	504.201 ± 1.26934	498.037 ± 1.47296
300 TeV	534.666 ± 1.1021	531.12 ± 1.2608

Table 3: The values for longitudinal depth at the maximum number of particles, X_{max}, for a Photon Primary Particle with different energies. Fitted with both the Gaisser-Hillas model and the Gaussian In Age model applied to the Full Shower Profile.

X_{max} Values Proton Primary Particle Full Shower Profile		
Energy	Gaisser-Hillas	Gaussian In Age
10 TeV	432.146 ± 3.26713	431.869 ± 3.34245
50 TeV	483.979 ± 3.0858	481.77 ± 3.18486
100 TeV	495.01 ± 2.59792	492.569 ± 2.69774
300 TeV	530.497 ± 2.65193	529.203 ± 2.7516

Table 4: The values for longitudinal depth at the maximum number of particles, X_{max}, for an Proton Primary Particle with different energies. Fitted with both the Gaisser-Hillas model and the Gaussian In Age model applied to the Full Shower Profile.